Gondwana Research 47 (2017) 249–266

Contents lists available at ScienceDirect

Gondwana Research

journal homepage: www.elsevier.com/locate/gr

Heterogeneous distribution of water in the mantle beneath the central Siberian Craton: Implications from the Udachnaya Kimberlite Pipe

Maria V. Kolesnichenko [a,*], Dmitry A. Zedgenizov [a,b], Konstantin D. Litasov [a,b], Inna Yu. Safonova [a,b], Alexey L. Ragozin [a,b]

[a] Sobolev Institute of Geology and Mineralogy, SB RAS, Koptyuga ave. 3, Novosibirsk 630090, Russia
[b] Novosibirsk State University, Pirogova st. 2, Novosibirsk 630090, Russia

ARTICLE INFO

Article history:
Received 14 April 2016
Received in revised form 21 September 2016
Accepted 24 September 2016
Available online 20 October 2016

Handling Editor: M. Santosh

Keywords:
Peridotite xenolith
Nominally anhydrous minerals
Degree of deformation
Content of water
Metasomatism

ABSTRACT

The paper presents new petrographic, major element and Fourier transform infrared (FTIR) spectroscopy data and PT-estimates of whole-rock samples and minerals of a collection of 19 relatively fresh peridotite xenoliths from the Udachnaya kimberlite pipe, which were recovered from its deeper levels. The xenoliths are non-deformed (granular), medium-deformed and highly deformed (porphyroclastic, mosaic-porphyroclastic, mylonitic) lherzolites, harzburgite and dunite. The lherzolites yielded equilibration temperatures (T) and pressures (P) ranging from 913 to 1324 °C and from 4.6 to 6.3 GPa, respectively. The non-deformed and medium-deformed peridotites match the 35 mW/m^2 conductive continental geotherm, whereas the highly deformed varieties match the 45 mW/m^2 geotherm. The content of water spans 2 ± 1–95 ± 52 ppm in olivine, 1 ± 0.5–61 ± 9 ppm in orthopyroxene, and 7 ± 2–71 ± 30 ppm in clinopyroxene. The amount of water in garnets is negligible. Based on the modal proportions of mineral phases in the xenoliths, the water contents in peridotites were estimated to vary over a wide range from <1 to 64 ppm. The amount of water in the mantle xenoliths is well correlated with the deformation degree: highly deformed peridotites show highest water contents (64 ppm) and those medium-deformed and non-deformed contain ca. 1 ppm of H_2O. The high water contents in the deformed peridotites could be linked to metasomatism of relatively dry diamondiferous cratonic roots by hydrous and carbonatitic agents (fluids/melts), which may cause hydration and carbonation of peridotite and oxidation and dissolution of diamonds. The heterogeneous distribution of water in the cratonic mantle beneath the Udachnaya pipe is consistent with the models of mantle plume or veined mantle structures proposed based on a trace element study of similar xenolithic suits. Mantle metasomatism beneath the Siberian Craton and its triggered kimberlite magmatism could be induced by mantle enrichment in volatiles (H_2O, CO_2) supplied by numerous subduction zones which surrounded the Siberian continent in Neoproterozoic-Cambrian time.

1. Introduction

Water plays a key role in the evolution and dynamics of the Earth's interior. Water can drastically change physical and chemical properties of mantle minerals, for instance, affect the degree of their deformation and impact mantle rheology (Miller et al., 1987; Mei and Kohlstedt, 2000a, 2000b). Knowing the amount of water present in the mantle nominally anhydrous minerals (NAMs), e.g., olivine, orthopyroxene, clinopyroxene, has a potential meaning upon the whole cycle of hydrogen in the Earth (Peslier et al., 2002). There are two major ways for reconstructing deep mantle conditions: study of mantle xenoliths and high-PT experiments. Of special importance are deep mantle xenoliths, which can be rapidly transported by alkali magmas, primarily kimberlite and basalt, to the Earth's surface. Those xenoliths are "direct" samples of the deep mantle and those of garnet-bearing peridotites, often referred to as cratonic peridotites, probably "nipped" the lithospheric mantle. In addition, many scientists think that the content of water in peridotite xenoliths (lherzolite, harzburgite, dunite) reflects hydration conditions and patterns in the sublithospheric continental mantle (Xia et al., 2010; Hao et al., 2012, 2014; Denis et al., 2015; Hui et al., 2015; Peslier and Bizimis, 2015; Schmadicke et al., 2015; Hao et al., 2016).

Kimberlites are the deepest magmas accessible to our observation and study, which are thought to be generated at the base of the lithospheric mantle of ancient cratons at depths of 150–250 km or even deeper in the asthenosphere. Despite the sparse occurrence of kimberlites, those rocks are very important objectives of the study of Earth deep interior as they are can carry deepest mantle xenoliths and even diamonds directly to the surface. The most common type of kimberlite xenoliths is garnet-bearing peridotite (typically referred to as "garnet

* Corresponding author at: V.S. Sobolev Institute of Geology and Mineralogy, SB RAS, Koptyuga ave. 3, Novosibirsk 630090, Russia.
E-mail address: m.kolesnichenko@igm.nsc.ru (M.V. Kolesnichenko).

http://dx.doi.org/10.1016/j.gr.2016.09.011
1342-937X/

peridotite"). Cratonic peridotites are considered residues of high degree mantle melting and are characterized by low Al_2O_3 (1–3 wt.%) and CaO (0.5–2 wt.%) and high magnesium number (Mg# = 90–93). These geochemical features allow researchers to distinguished them from off-craton peridotites, which, in average, have higher Al_2O_3 (1–5 wt.%) and CaO (1–8 wt.%) contents and slightly lower Mg# (88–90) (e.g., Boyd, 1989; Walter, 1998; Pearson et al., 2003; Herzberg, 2004; Lee, 2006; Bernstein et al., 2007; Simon et al., 2007). The estimation of the melting conditions of residual peridotites is possible by comparing their major element and modal compositions with experimental data on the melting of fertile peridotites (e.g., Walter, 1998; Herzberg, 2004).

The issue of water content in NAMs from kimberlites and xenoliths has been discussed in numerous works, including those on minerals of xenoliths from kimberlites worldwide in general and the Yakutian diamondiferous province in particular (e.g., Kurosawa et al., 1997; Matsyuk et al., 1998; Kent and Rossman, 2002; Matsyuk and Langer, 2004; Mosenfelder et al., 2006; Peslier et al., 2008; Yang et al., 2008; Hao et al., 2012; Doucet et al., 2014; Hao et al., 2014; Ragozin et al., 2014a, 2014b; Hui et al., 2015; Novella et al., 2015; Peslier and Bizimis, 2015; Schmadicke et al., 2015; Hao et al., 2016; Jean et al., 2016; Taylor et al., 2016). There are many techniques to estimate and calculate water content in NAMs, however, the Fourier transform infrared (FTIR) spectroscopy is a commonly used method because of its high sensitivity permitting to trace amounts of water. Water contents have been also obtained from mantle-derived xenoliths hosted by alkali basalts from other intracontinental areas, e.g., in the North China Craton, where Meso-Cenozoic basalts carry variably hydrated mantle peridotites (Yang et al., 2008; Xia et al., 2010, 2013; Li et al., 2015; Hao et al., 2016). Xenoliths of the world known Udachnaya kimberlite pipe, which is located in the central part of the Siberian craton, have been studied before, in particular, for major and trace elements, to show the equilibration pressures and temperatures spanning wide ranges of 2–7 GPa and 700–1400 °C, respectively (e.g., Doucet et al., 2014; Agashev et al., 2013).

In this paper we present new data on the mineral composition and water content for a most representative collection of variably deformed but relatively fresh 19 xenoliths of deep-seated mantle peridotites (garnet lherzolite, garnet harzburgite and dunite) from the Udachnaya pipe and new estimates of pressure and temperature. For the first time, we consider the contents of water and related PT-parameters in a close link with different types of garnet lherzolites classified by the degree of deformation. We will discuss the contents of water in major rock-forming minerals (olivine, orthopyroxene and clinopyroxene) in comparison with those obtained from a different, but less representative, set of Udachnaya garnet peridotites (Koch-Muller et al., 2006; Doucet et al., 2014). Special foci will be given to (i) water content of variably deformed samples; (ii) correlation between the concentrations of water in rock-forming minerals and in whole-rock peridotites and the degree of their deformation; (iii) reconstruction of deep mantle processes controlling the hydration of the lowermost cratonic lithosphere beneath the Siberian craton; (iv) possible links between water content variations and mantle metasomatism beneath the Siberian Craton; (v) causes and geodynamic consequences of mantle metasomatism.

2. Geological setting

The Yakutian kimberlite or diamondiferous province hosting the Udachnaya kimberlite pipe is located in the central part of the Siberian craton (Fig. 1). The Siberian Craton is the largest Precambrian continental fragment of Asia. It is covered by Late Precambrian, Paleozoic, and Mesozoic sedimentary rocks of the Siberian Platform and surrounded by the Verkhoyansk, Baikal-Patom and Southern Taymir orogenic belts. The basement of the Siberian Craton of dominantly Archean age is exposed within the Anabar and Aldan shields and in several smaller uplifts between the south-western Siberian Craton and the Central Asian Orogenic Belt (Smelov and Timofeev, 2007; Turkina et al., 2012). The Yakutian kimberlites typically intrude Vendian, Cambrian and

Fig. 1. Location of the Udachnaya kimberlite pipe in the Siberian Craton and surrounding tectonic structures: Late Proterozoic orogenic belts and Phanerozoic Central Asian Orogenic Belt. The dark elements are for the exposed basement of the Siberian Craton: Aldan and Anabar shields and other outliers.

Ordovician carbonate sediments (Kopylova et al., 2013). Five stages of kimberlite magmatism, Late Ordovician, Late Silurian, Late Devonian, Triassic, and Late Jurassic-Early Cretaceous (Table 1), have been recognized in the Yakutian kimberlite province based on the $^{206}Pb/^{238}U$ zircon and perovskite ages obtained from kimberlites and surrounding alluvial deposits (Davis et al., 1980; Kinny et al., 1997) and on the Rb–Sr isochron ages obtained from phlogopite phenocrysts and whole-rock kimberlites (Agashev et al., 2004).

There are thousands of kimberlite bodies in the Yakutian diamondiferous province, but only few, e.g., Udachnaya, Mir, and Obnazhennaya, contain peridotite xenoliths suitable for petrologic and geochemical investigations (Sobolev, 1977; Howarth et al., 2014). The Udachnaya kimberlite pipe is located in the Daldyn-Alakit region of the Yakutian kimberlite province and is one of Siberia biggest industrial diamond mines. The pipe intrudes Cambrian sedimentary rocks, such as carbonates, mudstone, siltstone, sandstones and conglomerate (Kopylova et al., 2013), and consists of two conjugate bodies, Udachnaya-East and Udachnaya-West, which merge at a depth of about 250 m. According to different evaluations each body formed during 3 to 5 episodes of eruption (Khar'kiv et al., 1991; Zinchuk et al., 1993). The two bodies are both diamondiferous, however possess variable petrographic, mineralogical, and chemical features. The U-Pb dating of perovskite and Ar-Ar dating of phlogopite from Udachnaya-East and Udachnaya-West kimberlites yielded the ages of ca. 369–366 Ma and ca. 361–353 Ma, respectively, i.e. the eastern body intruded earlier than the western one. The ages obtained from the Udachnaya pipe are consistent with those obtained from other kimberlite pipes of the Daldyn-Alakit field (Table 1) and with the Late Devonian major stage of kimberlite magmatism of the whole Yakutian province (Davis et al., 1980; Kinny et al., 1997).

The samples under study are from the Udachnaya eastern body taken at levels of ca. 400–500 m in the mine. Udachnaya East consists of (older to younger) of kimberlite breccia with phenocrysts of diopside and phlogopite (Egorov et al., 1986), volcaniclastic kimberlite and dikes of monticellite-bearing kimberlite (Kornilova et al., 1998). The kimberlite body contains untypically fresh deformed lherzolites carrying low to high-chromium garnets. In addition, Udachnaya-East carries xenoliths of dunites harzburgites and, in subordinate amounts, garnet-free

Table 1
Major age constraints on the kimberlite magmatism and mantle metasomatism from the Daldyn-Alakit kimberlite district and other key areas of the Yakutian diamondiferous province[a].

Objective	Analyzed material	Host rock	Ages	Method	Stage	Reference
Festival'naya KP	Zircon	Kimberlite	358–344 Ma	U-Pb dating	Magmatism	Davis et al. (1980)
Udachnaya KP	Zircon	Kimberlite	330–385 Ma	Fission-track	Magmatism	Ilupin (1990)
Udachnaya-East KP	Perovskite	Kimberlite	367 ± 5	U-Pb dating		Kinny et al. (1997)
Udachnaya-West KP	Perovskite	Kimberlite	361 ± 4 to 353 ± 5 Ma	U-Pb dating	Magmatism	Kinny et al. (1997)
Polyarnaya KP	Perovskite	Kimberlite	357 ± 3	U-Pb dating	Magmatism	Kinny et al. (1997)
Dalnyaya KP	Perovskite	Kimberlite	355 ± 5	U-Pb dating	Magmatism	Kinny et al. (1997)
Mir KP	Zircon	Kimberlite	353.6 ± 2.5 Ma	U-Pb dating	Magmatism	Spetsius et al. (2002)
Komsomolskaya KP	Phlogopite	Kimberlite	358 Ma	Rb-Sr isochrone	Magmatism	Agashev et al. (2004)
	Whole-rock		357 Ma			
Placers from NE Siberian platform	Rutile	Diamond	356 ± 54 Ma	U-Pb dating	Magmatism	Afanas'ev et al. (2009)
Udachnaya-East KP	Phlogopite	Kimberlite	365.9 ± 3.8 Ma	$^{40}Ar/^{39}Ar$	Magmatism	Yudin et al. (2014)
	Perovskite	Kimberlite	369 ± 10 Ma	U-Pb dating		
Udachnaya-East KP	Rutile	Eclogite	420.4 ± 9.6 Ma	U-Pb dating	Metasomatism	Ragozin et al. (2014a, 2014b)

[a] Ordered by the year of publication. KP, kimberlite pipe.

lherzolites, pyroxenities and eclogites. The Udachnaya-West kimberlite contains abundant, but strongly altered, both deformed and granular, garnet-bearing lherzolites. The degree of the serpentinization of olivine in Udachnaya East decreases from 80 to 95% in the upper 400 m of the kimberlite to almost nil at depths larger than 400 m.

3. Methods

Mineralogical composition and modal abundances of major minerals in the samples under study as well as their textures were examined with a Zeiss Axioscope 40 optical polarizing petrographic microscope at various magnifications. The major element composition of minerals was determined with a JEOL JXA-8100 electron microprobe using an accelerating voltage of 15 kV and a current of2 15 nA in the Institute of Geology and Mineralogy SB RAS. The quality of analyses were controlled by natural and synthetic standards (olivine CH-1, garnet O-145, pyroxene BD). For the full protocol of X-ray electron probe microanalysis see (Lavrent'ev et al., 2015). Abundances of major elements in whole-rock peridotites (wt.%) were determined at the Analytical Centre of the Sobolev Institute of Geology and Mineralogy, Siberian Branch, Russian Academy of Sciences (IGM SB RAS, Novosibirsk, Russia). The concentrations of a set of major oxides were measured by an X-ray fluorescence (XRF) device CMP-25 according to a state standard of the USSR Ministry of Geology (GOST 41-08-212-82). Relative standard deviations (RSD) are within 5%, and totals were within 100 ± 1%.

The hydrogen contents of selected grains was determined by FTIR spectroscopy. The preparation of samples for FTIR included several stages. First, we selected most transparent fragments of minerals with no optically or macroscopically visible inclusions or cracks. Then, we determined the orientation of minerals by observing interference figures using a petrographic microscope. Finally, each fragment was fixed on a glass slide with Crystalbond thermoplastics and then double-side polished using abrasive clothes C600, C800, C1500 and C3000 and then diamond paste. The thickness of grains was measured with an A.D. Leveridge Electronic Gemstone Gauge Presidium. The thickness of transparent fragments varies from 60 to 700 μm.

The FTIR polarized spectra were recorded at room temperature using a BRUKER VERTEX 70 Spectrometer equipped with a HYPERION 2000 IR Microscope (with resolution of 4 cm^{-1}, 30–70 scans, aperture 50 × 50 μm). Polarized absorption measurements were carried out in a spectral range from 600 to 7000 cm^{-1}. The calculation of water content was done using the Beer–Lambert law: $A = \varepsilon \cdot t \cdot c$, where ε is the coefficient of molar absorption, t is the thickness of the plate and c is the concentration of absorbing species in the sample, which describes the linear relationship between absorbance and concentration. Thereby, the concentration of hydrogen can be calculated from the integral intensity of $c(H_2O) = bA/t$. The coefficient b is equal to 0.188 for olivine (Bell et al., 2003), 0.067 for orthopyroxene, 0.141 for clinopyroxene, and 0.24 for garnet (Bell et al., 1995). The published data used for comparison are available in Suppl. Electr. Mat.

Table 2
A summary of petrologic and water content data from the variably deformed Udachnaya peridotites.

No.	Sample	Rock type	Texture	Degree of deformation	Modal abundance, vol.%					Water content, ppm							T, °C	P, GPa
					Ol	Opx	Cpx	Grt	Chr	Ol	σ	Opx	σ	Cpx	σ	WR		
1	Ud-226-02	Grt-lhz	M-P	HD	60	25	5	10	–	67	49	31	17	42	3	50	1271	5.0
2	Ud-1-07	Grt-lhz	My	HD	50	25	15	10	–	53	34	33	9	71	30	45	1250	5.2
3	Ud-51-04	Grt-lhz	M-P	HD	45	20	20	15	–	95	52	8	2	59	13	56	1282	5.6
4	Ud-8-04	Grt-lhz	M-P	HD	60	25	5	10	–	43	2	13	2	29	7	31	1245	5.4
5	Ud-11-04	Grt-lhz	M-P	HD	70	15	5	10	–	83	18	23	13	39	16	64	1320	4.8
6	Ud-195-02	Grt-lhz	M-P	HD	60	10	15	15	–	62	34	61	9	38	2	49	1324	5.3
7	Ud-998-05	Grt-lhz	M-P	HD	45	20	25	10	–	19	6	21	15	41	2	23	1285	5.1
8	Ud-17-04	Grt-lhz	P	MD	50	30	10	10	–	7	17	28	5	27	7	15	1306	5.3
9	Ud-602	Grt-lhz	P	MD	50	30	10	10	–	11	12	30	2	25	6	17	1211	5.3
10	Ud-35-02	Grt-lhz	P	MD	45	20	10	25	–	12	7	17	7	43	10	13	960	6.3
11	Ud-211-02	Grt-lhz	P	MD	45	25	10	20	–	22	9	20	17	39	9	19	1312	4.8
12	Ud-8-07	Grt-lhz	P	MD	70	10	5	15	–	8	7	11	1	32	9	8	1291	5.1
13	Ud-75-04	Grt-lhz	P	MD	55	30	5	10	–	4	1	27	22	7	2	11	1295	4.7
14	Ud-334-05	Grt-lhz	P	MD	65	25	5	5	–	20	11	42	26	41	5	26	1322	4.6
15	Ud-10-04	Grt-lhz	G	ND	50	20	15	15	–	5	4	21	4	29	2	11	1039	5.9
16	Ud-21-07	Lhz	G	ND	70	20	5	-	5	5	2	17	4	32	17	9	913	5.3
17	Ud-6-07	Grt-lhz	G	ND	45	10	20	25	–	9	5	0	-	21	6	8	976	5.2
18	Ud-28-07	Grt-hrz	G	ND	50	40	–	10	–	2	1	1	0.5	-	-	1	962	5.0
19	Ud-60-02	Dunite	G	ND	95	–	–	–	5	2	1	–	–	–	–	2	–	–

Abbreviations: Grt-lhz, garnet lherzolite; Lhz, lherzolite; Grt-hrz, garnet harzburgite; WR, whole-rock; M-P, mosaic-porphyroclastic; P, porphyroclastic; My, mylonitic; G, granular; σ, standard deviation. The temperature and pressure estimates are after (Brey and Koehler, 1990) and (Koehler and Brey, 1990), respectively.

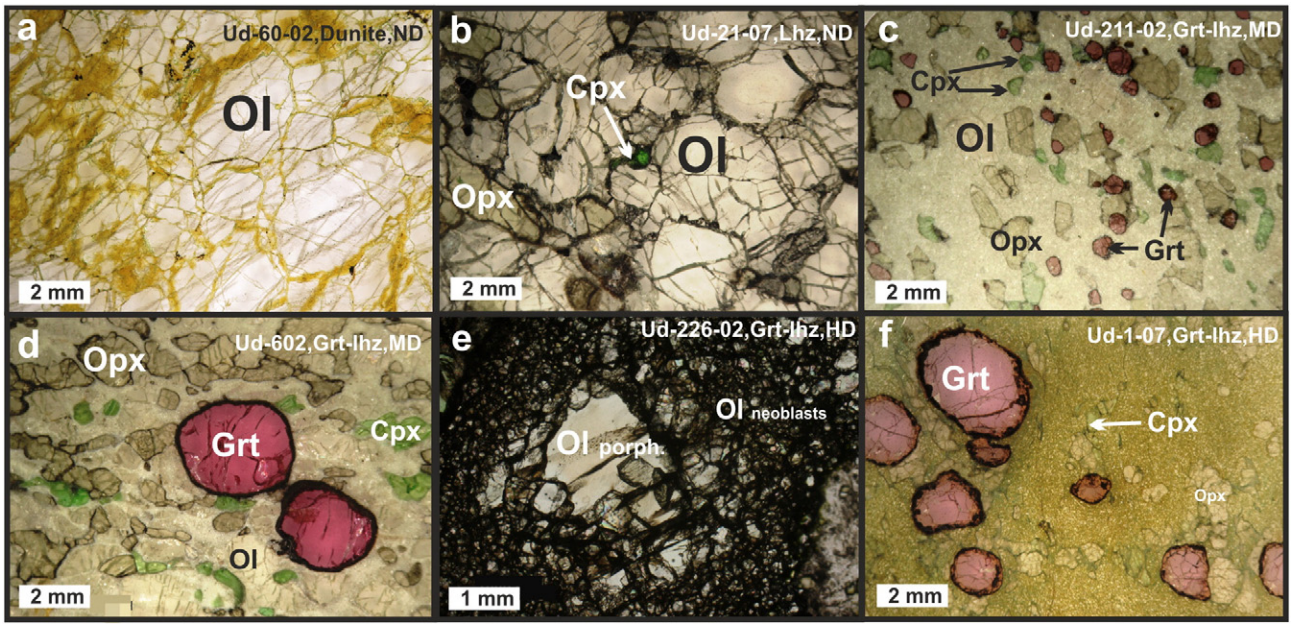

Fig. 2. Optical microscopy photos of Udachnaya peridotite xenoliths. Textures: a, b – granular; c, d – porphyroclastic; e - mosaic-porphyroclastic; f – mylonitic. Cpx, clinopyroxene; Grt, garnet; Lhz, lherzolite; Grt-lhz, garnet lherzolite; Ol, olivine; Opx, orthopyroxene.

4. Petrography and mineral composition of mantle xenoliths

Nineteen peridotite xenoliths including 16 garnet lherzolites plus 3 samples of garnet harzburgite, garnet-free lherzolite and dunite, were selected for our study. Mineral composition and major petrographic features of rocks are summarized in Table 2 and illustrated in Figs. 2 and 3. The major group of garnet lherzolites is characterized by 45–70% olivine (Ol), 10–40% orthopyroxene (Opx), 5–25% clinopyroxene (Cpx) and

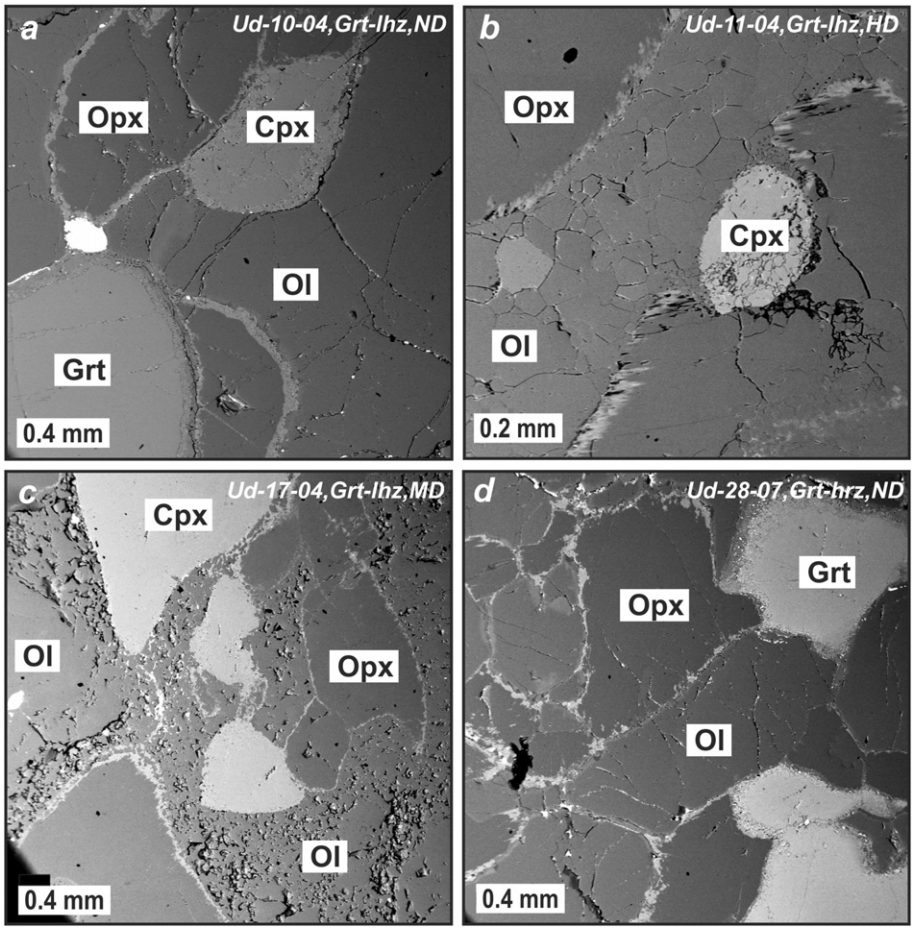

Fig. 3. Photomicrographs of Udachnaya peridotites. Samples: a, d – non-deformed; b – highly deformed; c – medium-deformed.

10–25% garnet (Grt). The modal mineral compositions of the samples see in Table 2. Texturally, we divided the samples into three groups based on the degree of deformation: granular or non-deformed lherzolites, harzburgite and dunite (ND), medium-deformed lherzolites (MD) and highly deformed lherzolites (HD) (Fig. 2).

Peridotite xenoliths have typically granular, moderately deformed (porphyroclastic) and strongly sheared (mosaic-porphyroclastic and mylonitic) textures (Harte, 1977; Passchier and Trouw, 2005). Among the samples under investigation, the deformed samples consist of porphyroclasts submerged into a matrix of fine-grained olivine (Fig. 2c–f). The degrees of deformation, the proportions of porphyroclasts and their sizes, and, consequently, the microstructures are extremely variable. The size of porphyroclasts ranges from 1 to 4 mm in diameter. The rocks display transitions from non-deformed granular microstructures to highly deformed strongly sheared (mylonitic) microstructures.

The Udachnaya granular lherzolites and garnet harzburgite (ND) have protogranular coarse-grained microstructures (Figs. 2b, 3a, d). Olivine and orthopyroxene have similar shapes, but Opx grains are larger than those of Ol. Moreover, Ol grains in sample Ud-21-07 are irregularly elongated; Opx grains are often cracked and clinopyroxene occurs as small anhedral interstitial crystals. Garnet grains are isometrically shaped and often surrounded by kelyphitic rims (Fig. 2b). The Udachnaya medium-deformed (MD) garnet lherzolites possess moderately deformed (porphyroclastic) textures (Figs. 2c, d, 3c). Olivine grains occur as porphyroclasts and neoblasts. Several large Ol grains are surrounded by anhedral neoblasts of olivine. Clinopyroxenes also have anhedral shapes. In several samples Opx grains show cracks (Ud-602; Fig. 2d). The shape of garnet grains is isometric. The textures in the highly deformed garnet lherzolites (HD) of the Udachnaya-East vary from mosaic-porphyroclastic to mylonitic. Olivines are dilapidated (tumble-down) and surrounded by euhedral olivine neoblasts which form a mosaic matrix. The only sample of dunite (Fig. 2a) represents a coarse-grained megacrystalline rock with granular reticulate microstructure. It consists of olivine (95 vol.%), which grains are surrounded by secondary serpentine rims and primary chromite (up to 5 vol.%).

5. Results

5.1. Whole-rock composition of Udachnaya xenoliths

Whole-rock major element compositions are shown in Table 3. All peridotite samples are depleted in magmaphile elements and plot between the compositional point of Bulk Silicate Earth (BSE) (McDonough and Sun, 1995) and cratonic peridotite (McDonough and Rudnick, 1998) in the co-variation diagrams of CaO, Al_2O_3 and MnO vs. MgO suggesting their residual nature (Fig. 4). The samples are characterized by typical high MgO (39.37–47.29) and Mg# (94.7–95.7), but show a wider range of SiO_2 (38.2–43.85 wt.%) compared to previously published data (Agashev et al., 2013). Several peridotite samples show weak enrichments in CaO and K_2O. The contents of MgO are negatively correlated with Al_2O_3, CaO, and MnO (Fig. 4a, b, d). FeO and K_2O in the deformed peridotites show no mutual correlations, but increase with increasing as TiO_2 and CaO, respectively (Fig. 4e, f). This suggests that the enrichment of the peridotites in FeO and K_2O resulted from different processes. Seven variably deformed samples have negative losses of ignition (LOI) probably due to the oxidation of FeO to Fe_2O_3, which is consistent with their fresh appearance (Agashev et al., 2013). The other samples have positive LOI values ranging from 0 to 1.5 wt.%. Four samples can be considered as altered by the presence of brucite or other secondary water-bearing minerals and their as their LOI values are very high: from 4.2 to 8.4 wt.% (Table 3). Our sample set shows weak to medium correlations between LOI and CaO and FeO (not shown here), similarly to the sample suite of Boyd et al. (1997), in which those correlations were well documented to reveal significant sub-surface alteration.

5.2. Mineral compositions

Tables 4-7 show summarized compositions of rock-forming minerals. Olivines are compositionally close to “pure” forsterite with Mg# ranging from 90.8 to 92.4 (Table 4), i.e., higher than those reported before: 86.4–91.3 in (Agashev et al., 2013) and 85.4–91.8 in (Sobolev et al., 2009), but similar to those reported by (Doucet et al., 2014). Our data on the MnO content in olivines are consistent with those reported by (Sobolev et al., 2009). All the peridotites under study showing different degrees of deformation plot close to the intersection of coarse-grained and high-deformed peridotite fields (Fig. 5a, b).

Fig. 6a shows three clusters of compositions: for garnet, Cpx and Opx The Mg# value of orthopyroxenes ($100 \times Mg/(Mg + Fe)$) ranges from 89.2 to 93.5 (Fig. 6b) and the Al_2O_3 content varies from 0.4 to 0.6 wt.% (Table 5). Several orthopyroxene grains, from non to highly deformed xenoliths, have high concentrations of CaO (0.9–1.2 wt.%)). The selected Udachnaya clinopyroxenes are typically Cr-diopsides (Fig. 6b). They have Mg# = 87.4–95.3 and contain Cr_2O_3 = 0.8–2.2 wt.%. The Ca# ($100 \times Ca/(Ca + Mg)$) value spans 39.5 to 48.1 (Table 6).

The garnets are characterized by variable Cr_2O_3 (1.65–8.63 wt.%) and CaO (4.33–6.48 wt.%) and less variable MgO (Table 7; Figs. 6a, 7). The positive correlation between CaO and Cr_2O_3 corresponds to the lherzolitic trend (Sobolev et al., 1973) and to the successions reported by (Agashev et al., 2013; Doucet et al., 2014; Howarth et al., 2014) (Fig. 7). The full set of more than 170 microprobe analyses of olivine,

Table 3
Whole-rock major elements of Udachnaya peridotite xenoliths.

No.	Sample	SiO_2	TiO_2	Al_2O_3	FeO*	MnO	MgO	CaO	Na_2O	K_2O	P_2O_5	Cr_2O_3	NiO	Sum	LOI	Mg#
1	Ud-226-02	42.58	0.09	0.95	8.93	0.12	45.43	1.12	0.11	0.09	0.02			99.18	−0.27	95.3
2	Ud-1-07	43.73	0.11	1.78	8.75	0.12	42.81	1.59	0.11	0.16	0.02			99.65	0.47	95.1
3	Ud-51-04	42.85	0.12	1.84	9.36	0.13	42.53	1.77	0.27	0.15	0.02			99.66	0.61	94.7
4	Ud-8-04	41.61	0.13	1.06	9.37	0.12	46.18	0.89	0.15	0.10	0.04	0.25	0.33	100.19	−0.08	96.7
5	Ud-11-04	43.85	0.11	2.22	8.85	0.14	40.87	2.44	0.20	0.17	0.02			99.39	0.51	98.6
6	Ud-195-02	42.14	0.09	1.78	8.81	0.13	44.84	1.72	0.18	0.16	0.02			99.47	−0.41	98.1
7	Ud-998-05	41.37	0.10	1.05	9.75	0.12	45.56	1.12	0.13	0.10	0.03	0.16	0.33	99.79	−0.11	97.4
8	Ud-17-04	43.04	0.02	1.32	9.12	0.13	43.99	1.61	0.13	0.12	0.02			99.51	0.00	98.1
9	Ud-35-02	44.14	0.30	8.63	7.16	0.18	29.07	4.22	0.27	0.55	0.07	1.23	0.07	100.30	4.24	98.9
10	Ud-211-02	41.27	0.06	0.62	9.38	0.11	47.29	0.93	0.08	0.06	0.03	0.14	0.35	100.13	−0.30	97.0
11	Ud-8-07	38.63	0.14	0.85	10.98	0.11	38.97	0.89	0.07	0.09	0.03	0.28	0.28	99.97	8.38	97.0
12	Ud-75-04	42.13	0.05	0.66	8.92	0.12	46.36	1.03	0.12	0.14	0.03	0.19	0.33	99.87	−0.27	97.2
13	Ud-334-05	42.22	0.08	0.71	9.24	0.11	46.09	0.98	0.11	0.08	0.04	0.25	0.33	100.35	0.04	97.2
14	Ud-10-04	42.13	0.13	2.97	8.76	0.13	41.33	2.57	0.31	0.42	0.02			99.38	0.60	98.8
15	Ud-21-07	39.23	0.16	0.56	8.89	0.11	46.38	1.72	0.05	0.15	0.06	0.45	0.30	99.63	1.26	98.4
16	Ud-6-07	38.96	0.20	1.90	8.41	0.11	39.37	1.99	0.14	0.32	0.05	0.17	0.27	99.68	7.39	98.6
17	Ud-28-07	40.58	0.07	1.52	9.15	0.12	46.10	1.31	0.08	0.23	0.04	0.48	0.34	100.06	−0.18	97.8
18	Ud-60-02	38.21	0.04	0.27	8.02	0.10	45.34	0.27	0.02	0.04	0.02	0.13	0.38	100.02	7.09	91.2

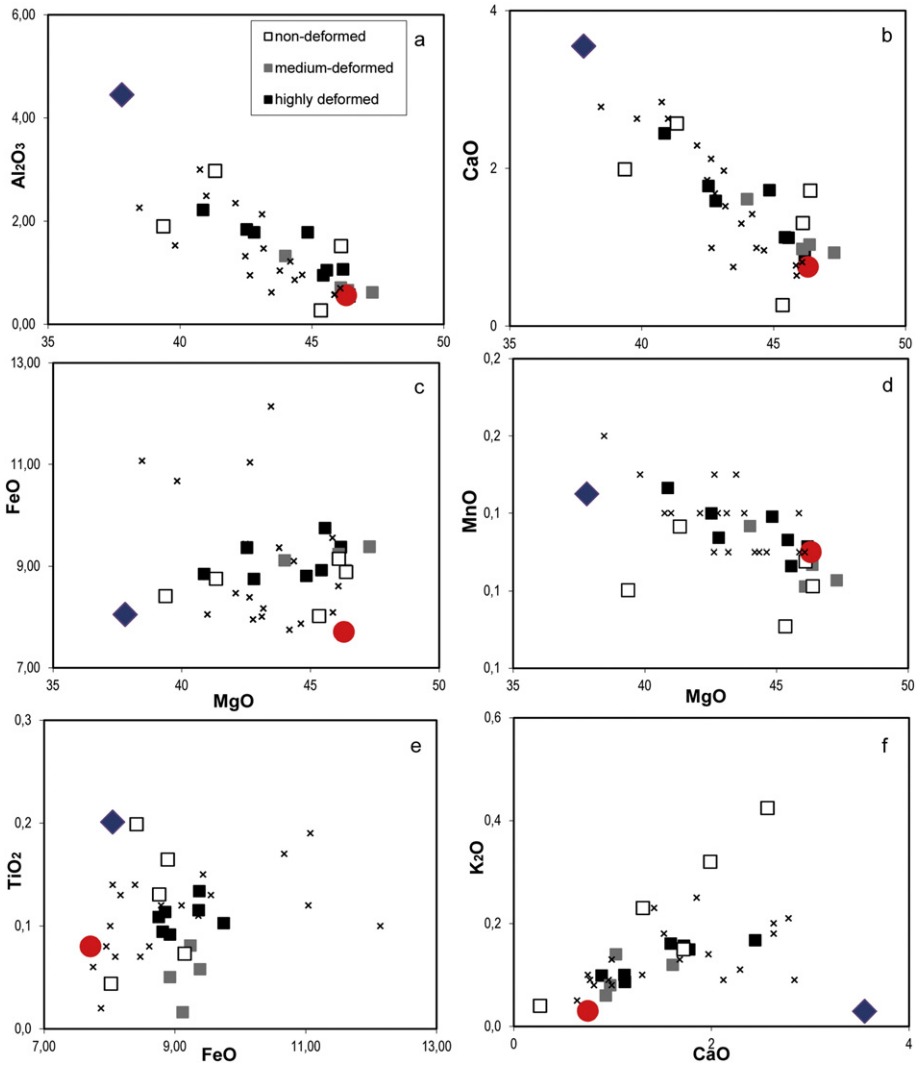

Fig. 4. Binary plots for whole rocks major oxides. Squares for Udachnaya peridotites: empty – non-deformed, gray – medium-deformed, black – highly deformed. Data sources: Agashev et al., 2013 (crosses) for Udachnaya peridotites; McDonough and Sun, 1995 (red circles) for the primitive mantle; McDonough and Rudnick, 1998 (blue diamonds) for cratonic harzburgite.

orthopyroxene, clinopyroxene and garnet is available as e-component (supplementary materials).

5.3. Pressure and temperature (P-T) estimates

We calculated the equilibration conditions for Udachnaya peridotites by the solvus isotherms for coexisting Opx and Cpx and by the Ca partitioning between Ol and Cpx (Brey and Koehler, 1990). Our obtained results we compared with those from the previous studies (Agashev et al., 2013; Doucet et al., 2014; Howarth et al., 2014). The calculated temperature and pressure estimates are given in Table 2 and illustrated in Fig. 8. The P_{BK90}-T_{BK90} (pressures and temperatures estimated by the Brey&Kohler and Kohler&Brey geobarometer and geothermometer, respectively) define a broad P-T range from 4.6 to 6.3 GPa and from 913 to 1324 °C for all peridotites. The non-deformed and medium-deformed peridotites formed at 5.0–6.3 GPa and 913–1039 °C. This range of relatively low-temperature rocks matches the 35 mW/m^2 conductive continental geotherm. The temperature estimates from the highly deformed peridotites are notably higher ranging from 1245 to 1324 °C. So, the highly deformed peridotites correspond to the 45 mW/m^2 conductive continental geotherm. Our PT-estimates are consistent with those obtained by previous studies. For example, Doucet et al. (2014) obtained the estimates of 2.2–6.9 GPa and 735–1289 °C for coarse-grained peridotites and 6.3–6.6 GPa and 1281–1341 °C for sheared peridotites. The samples of peridotites studied by Agashev et al. (2013) and Howarth et al. (2014) form a compact PT-field in the PT-diagram, which is located between the 40 and 45 mW/m^2 geotherms (Fig. 8).

5.4. FTIR spectra

Over 120 grains of olivine, garnet and both pyroxenes separated from 19 samples were analyzed by FTIR, providing estimates of hydroxyl distributions and concentrations in nominally anhydrous minerals from all three groups (non-deformed, medium-deformed and highly deformed; see Table 2 and Figs. 2, 3) of Udachnaya peridotite xenoliths. Table 2 shows water concentrations as averages from several grains. Garnet grains are very clear and large, up to 6 mm in diameter (Fig. 2e, f). Their FTIR spectra do not show water absorption bands suggesting a detection limit of 0.5 ppm wt. H_2O. They are hence considered anhydrous.

5.4.1. Olivine

The spectra of all olivine samples show OH stretching bands in the range of 3700–3100 cm^{-1} with variable absorption intensities. All bands are characterized by a strong anisotropy, demonstrating that

Table 4
Chemical compositions of olivines from Udachnaya pipe xenoliths.

No.	Sample		SiO_2	Cr_2O_3	MnO	FeO	MgO	CaO	NiO	Total	Mg#
1	Ud-226-02	n = 6	41.4	0.04	0.1	8.7	50.4	0.04	0.3	101.1	91.1
		σ	0.1	0.01	0.0	0.0	0.1	0.00	0.0	0.2	
2	Ud-1-07	n = 1	41.0	0.03	0.1	8.9	50.1	0.04	0.4	100.6	90.9
3	Ud-51-04	n = 8	41.4	0.03	0.1	8.7	50.3	0.03	0.4	101.0	91.2
		σ	0.2	0.01	0.0	1.0	0.8	0.02	0.0	0.2	
4	Ud-8-04	n = 6	41.0	0.04	0.1	8.6	49.6	0.04	0.4	99.7	91.1
		σ	0.1	0.01	0.0	0.0	0.2	0.00	0.0	0.3	
5	Ud-11-04	n = 11	41.2	0.04	0.1	9.0	50.1	0.04	0.4	100.9	90.8
		σ	0.2	0.00	0.0	0.1	0.1	0.00	0.0	0.3	
6	Ud-195-02	n = 15	41.1	0.03	0.1	8.6	50.1	0.04	0.3	100.4	91.2
		σ	0.1	0.00	0.0	0.0	0.1	0.00	0.0	0.2	
7	Ud-998-05	n = 1	40.8	0.01	0.1	9.4	49.0	0.04	0.4	99.7	90.3
8	Ud-17-04	n = 15	41.0	0.03	0.1	8.8	49.9	0.04	0.4	100.3	91.0
		σ	0.1	0.00	0.0	0.0	0.2	0.00	0.0	0.2	
9	Ud-602	n = 13	41.2	0.03	0.1	8.9	50.0	0.04	0.4	100.6	91.0
		σ	0.1	0.00	0.0	0.1	0.1	0.00	0.0	0.2	
10	Ud-35-02	n = 6	41.0	0.01	0.1	7.9	50.2	0.01	0.3	99.5	91.9
		σ	0.1	0.01	0.0	0.1	0.2	0.00	0.0	0.2	
11	Ud-211-02	n = 7	41.0	0.04	0.1	8.9	49.3	0.05	0.4	99.8	90.8
		σ	0.1	0.01	0.0	0.0	0.2	0.01	0.0	0.2	
12	Ud-8-07	n = 5	41.1	0.02	0.1	7.5	50.3	0.02	0.4	99.4	92.3
		σ	0.1	0.02	0.0	0.5	0.3	0.01	0.0	0.2	
13	Ud-75-04	n = 8	41.0	0.05	0.1	8.5	49.6	0.05	0.4	99.7	91.2
		σ	0.2	0.00	0.0	0.0	0.2	0.00	0.0	0.3	
14	Ud-334-05	n = 7	41.0	0.05	0.1	8.7	49.7	0.05	0.4	100.0	91.1
		σ	0.3	0.01	0.0	0.0	0.1	0.00	0.0	0.4	
15	Ud-10-04	n = 12	41.2	0.01	0.1	8.3	50.4	0.01	0.3	100.4	91.6
		σ	0.1	0.00	0.0	0.0	0.1	0.00	0.0	0.2	
16	Ud-21–07	n = 7	41.2	0.01	0.1	7.4	50.5	0.01	0.3	99.6	92.4
		σ	0.3	0.00	0.0	0.0	0.2	0.00	0.0	0.5	
17	Ud-6-07	n = 6	41.1	0.01	0.1	8.3	50.0	0.01	0.3	99.8	91.5
		σ	0.1	0.01	0.0	0.0	0.2	0.00	0.0	0.2	
18	Ud-28–07	n = 7	41.2	0.01	0.1	8.1	50.0	0.01	0.4	99.8	91.7
		σ	0.1	0.01	0.0	0.0	0.1	0.00	0.0	0.2	
19	Ud-60-02	n = 9	41.1	0.00	0.1	7.6	50.3	0.01	0.3	99.5	92.2
		σ	0.3	0.00	0.0	0.1	0.2	0.00	0.0	0.4	

Hereinafter, we show average values and standard deviations (σ); n, number of measurements. The full set of analytical data is available in Suppl. Electr. Mat.

Table 5
Chemical compositions of orthopyroxenes from Udachnaya pipe xenoliths.

No.	Sample		SiO_2	TiO_2	Al_2O_3	Cr_2O_3	MnO	FeO	MgO	CaO	Na_2O	K_2O	Total	Mg#
1	Ud-226-02	n = 7	57.8	0.1	0.5	0.3	0.1	5.1	34.9	0.7	0.2	0.0	99.7	92.4
		σ	0.1	0.0	0.0	0.0	0.0	0.1	0.2	0.0	0.0	0.0	0.2	
2	Ud-1-07	n = 10	58.3	0.1	0.5	0.2	0.1	5.3	34.9	0.7	0.1	0.0	100.2	92.2
		σ	0.2	0.0	0.0	0.0	0.0	0.1	0.1	0.1	0.0	0.0	0.2	
3	Ud-51-04	n = 7	58.1	0.1	0.6	0.2	0.1	5.4	34.7	0.8	0.2	0.0	100.2	92.0
		σ	0.2	0.0	0.0	0.0	0.0	0.1	0.1	0.0	0.0	0.0	0.3	
4	Ud-8-04	n = 2	57.5	0.1	0.5	0.3	0.1	5.0	35.3	0.7	0.1	0.0	99.7	92.6
5	Ud-11-04	n = 6	57.8	0.2	0.6	0.3	0.1	5.3	34.8	0.9	0.2	0.0	100.2	92.2
		σ	0.2	0.0	0.0	0.0	0.0	0.1	0.2	0.0	0.0	0.0	0.4	
6	Ud-195-02	n = 2	58.2	0.1	0.5	0.2	0.1	4.9	34.6	0.7	0.2	0.0	99.6	92.6
7	Ud-998-05	n = 7	58.0	0.2	0.6	0.2	0.1	5.5	34.3	0.8	0.2	0.0	99.8	91.8
		σ	0.4	0.0	0.0	0.0	0.0	0.1	0.2	0.1	0.0	0.0	0.4	
8	Ud-17-04	n = 10	58.2	0.0	0.4	0.2	0.1	5.1	34.9	0.7	0.1	0.0	99.9	92.4
		σ	0.2	0.0	0.0	0.0	0.0	0.0	0.1	0.0	0.0	0.0	0.2	
9	Ud-602	n = 9	58.0	0.0	0.5	0.2	0.1	5.1	34.7	0.7	0.1	0.0	99.4	92.4
		σ	0.2	0.0	0.0	0.0	0.0	0.0	0.1	0.0	0.0	0.0	0.3	
10	Ud-35-02	n = 7	58.0	0.1	0.4	0.2	0.1	4.6	36.4	0.3	0.1	0.0	100.1	93.4
		σ	0.1	0.0	0.0	0.0	0.0	0.1	0.2	0.0	0.0	0.0	0.3	
11	Ud-211-02	n = 7	58.3	0.1	0.6	0.3	0.1	5.2	34.5	0.9	0.2	0.0	100.2	92.2
		σ	0.1	0.0	0.0	0.0	0.0	0.0	0.1	0.0	0.0	0.0	0.2	
12	Ud-8-07	n = 7	57.1	0.2	0.6	0.2	0.1	7.2	33.4	0.9	0.2	0.0	100.0	89.2
		σ	0.2	0.0	0.0	0.0	0.0	0.1	0.1	0.0	0.0	0.0	0.2	
13	Ud-75-04	n = 7	58.4	0.0	0.5	0.3	0.1	4.9	34.7	0.9	0.1	0.0	99.9	92.7
		σ	0.2	0.0	0.0	0.0	0.0	0.0	0.1	0.0	0.0	0.0	0.3	
14	Ud-334-05	n = 6	57.7	0.1	0.5	0.3	0.1	5.1	34.9	1.2	0.2	0.1	100.1	92.5
		σ	0.5	0.0	0.0	0.0	0.0	0.1	0.3	0.2	0.1	0.1	0.5	
15	Ud-10-04	n = 8	58.1	0.1	0.5	0.2	0.1	4.9	35.3	0.3	0.1	0.0	99.5	92.8
		σ	0.3	0.0	0.0	0.0	0.0	0.0	0.2	0.0	0.0	0.0	0.3	
16	Ud-21–07	n = 6	58.1	0.0	0.6	0.3	0.1	4.5	36.1	0.3	0.1	0.0	100.0	93.5
		σ	0.1	0.0	0.0	0.0	0.0	0.0	0.2	0.0	0.0	0.0	0.2	
17	Ud-28–07	n = 5	55.0	0.0	0.5	0.2	0.1	5.4	38.3	0.3	0.1	0.0	100.0	92.6
		σ	7.8	0.0	0.3	0.1	0.0	1.4	6.6	0.2	0.0	0.0	0.4	

Table 6
Chemical compositions of clinopyroxenes from Udachnaya pipe xenoliths.

No.	Sample		SiO_2	TiO_2	Al_2O_3	Cr_2O_3	FeO	MnO	MgO	CaO	K_2O	Na_2O	Total	Ca#	Mg#
1	Ud-226-02	n = 10	55.2	0.3	1.3	1.5	3.0	0.1	18.4	18.0	0.0	1.7	99.5	41.2	91.7
		σ	0.2	0.0	0.2	0.0	0.1	0.0	0.1	0.4	0.0	0.1	0.3		
2	Ud-1-07	n = 14	55.3	0.3	1.4	1.0	3.0	0.1	18.7	18.7	0.0	1.4	100.0	41.8	91.6
		σ	0.1	0.0	0.1	0.0	0.1	0.0	0.1	0.3	0.0	0.1	0.2		
3	Ud-51-04	n = 14	55.3	0.3	1.4	1.0	3.2	0.1	18.6	18.0	0.1	1.5	99.4	41.1	91.1
		σ	0.5	0.0	0.1	0.1	0.3	0.0	0.2	0.6	0.1	0.1	0.4		
4	Ud-8-04	n = 8	54.9	0.1	1.0	1.2	3.0	0.1	18.7	18.9	0.0	1.3	99.4	42.0	91.8
		σ	0.2	0.0	0.1	0.1	0.1	0.0	0.1	0.4	0.0	0.1	0.3		
5	Ud-11-04	n = 9	55.2	0.4	1.7	1.0	3.4	0.1	18.9	17.2	0.0	1.7	99.7	39.6	90.8
		σ	0.2	0.0	0.0	0.2	0.1	0.0	0.2	0.2	0.0	0.1	0.3		
6	Ud-195-02	n = 14	55.4	0.2	1.1	0.9	2.8	0.1	18.6	19.0	0.0	1.3	99.5	42.4	92.1
		σ	0.3	0.1	0.2	0.1	0.2	0.0	0.2	0.5	0.1	0.2	0.3		
7	Ud-998-05	n = 12	55.6	0.3	1.6	1.0	3.3	0.1	18.7	18.0	0.0	1.5	100.2	40.9	90.9
		σ	0.2	0.1	0.1	0.1	0.1	0.0	0.3	0.2	0.0	0.1	0.3		
8	Ud-17-04	n = 9	55.5	0.0	0.9	1.0	2.7	0.1	18.8	19.4	0.0	1.0	99.5	42.6	92.5
		σ	0.2	0.0	0.0	0.0	0.1	0.0	0.2	0.2	0.0	0.0	0.1		
9	Ud-602	n = 15	55.4	0.0	0.9	1.0	2.7	0.1	18.9	19.9	0.0	1.0	100.1	43.1	92.5
		σ	0.2	0.0	0.1	0.0	0.1	0.0	0.2	0.5	0.0	0.1	0.2		
10	Ud-35-02	n = 7	55.0	0.2	2.2	1.5	1.8	0.1	16.3	20.4	0.0	2.0	99.5	47.4	94.1
		σ	0.3	0.0	0.0	0.1	0.0	0.0	0.1	0.1	0.0	0.0	0.4		
11	Ud-211-02	n = 11	55.9	0.1	1.2	0.8	3.2	0.1	19.5	18.2	0.0	1.1	100.1	40.1	91.6
		σ	0.3	0.0	0.0	0.1	0.0	0.0	0.2	0.2	0.0	0.0	0.3		
12	Ud-8-07	n = 8	54.6	0.3	1.5	1.2	4.6	0.1	18.1	17.0	0.0	1.8	99.2	40.4	87.4
		σ	0.3	0.0	0.1	0.2	0.1	0.0	0.2	0.3	0.0	0.1	0.2		
13	Ud-75-04	n = 11	55.8	0.0	0.8	1.0	2.8	0.1	19.8	19.0	0.1	0.7	100.2	40.9	92.7
		σ	0.1	0.0	0.0	0.0	0.0	0.0	0.1	0.1	0.0	0.0	0.2		
14	Ud-334-05	n = 3	55.1	0.1	0.9	1.0	3.2	0.1	20.0	18.2	0.1	0.9	99.5	39.5	91.7
		σ	0.3	0.0	0.0	0.0	0.0	0.0	0.2	0.0	0.0	0.0	0.3		
15	Ud-10-04	n = 11	55.5	0.3	3.2	1.5	2.0	0.1	15.5	18.7	0.0	2.8	99.6	46.5	93.2
		σ	0.3	0.0	0.1	0.1	0.0	0.0	0.2	0.2	0.0	0.1	0.3		
16	Ud-21–07	n = 6	55.1	0.0	1.9	2.2	1.6	0.1	16.2	20.8	0.0	1.9	99.8	48.0	94.7
		σ	0.2	0.0	0.0	0.0	0.0	0.0	0.1	0.1	0.0	0.0	0.4		
17	Ud-6-07	n = 10	55.1	0.2	2.7	0.8	1.9	0.1	16.2	20.7	0.0	2.0	99.6	47.9	93.9
		σ	0.2	0.0	0.0	0.0	0.0	0.0	0.1	0.1	0.0	0.0	0.3		
18	Ud-28–07	n = 1	55.6	0.0	1.2	1.2	1.5	0.1	17.4	22.4	0.1	0.9	100.4	48.1	95.3

Table 7
Chemical compositions of garnets from Udachnaya pipe xenoliths.

No.	Sample		SiO_2	TiO_2	Al_2O_3	Cr_2O_3	MgO	MnO	FeO	CaO	Na_2O	Total
1	Ud-226-02	n = 6	41.12	0.26	16.37	8.62	19.46	0.36	7.11	6.12	0.05	99.48
		σ	0.09	0.14	0.19	0.13	0.06	0.01	0.07	0.04	0.02	0.16
2	Ud-1-07	n = 11	41.72	0.36	19.65	4.24	20.77	0.34	7.49	4.94	0.05	99.57
		σ	0.11	0.08	0.08	0.09	0.11	0.01	0.05	0.03	0.01	0.20
3	Ud-51-04	n = 10	41.92	0.36	19.78	4.07	20.79	0.35	7.60	4.78	0.07	99.72
		σ	0.16	0.02	0.08	0.06	0.07	0.01	0.05	0.03	0.01	0.15
4	Ud-8-04	n = 8	40.95	0.18	16.64	8.31	19.41	0.39	7.45	6.27	0.03	99.63
		σ	0.27	0.01	0.12	0.17	0.48	0.01	0.04	0.06	0.00	0.46
5	Ud-11-04	n = 16	41.11	0.19	17.72	6.86	20.09	0.33	7.14	5.88	0.05	99.37
		σ	0.25	0.13	0.10	0.13	0.07	0.01	0.05	0.06	0.02	0.27
6	Ud-195-02	n = 8	41.62	0.25	19.67	4.45	20.65	0.36	7.33	5.06	0.05	99.44
		σ	0.23	0.01	0.16	0.11	0.06	0.01	0.04	0.04	0.01	0.25
7	Ud-998-05	n = 6	42.11	0.20	20.27	3.74	21.16	0.33	7.73	4.49	0.05	100.09
		σ	0.32	0.05	0.14	0.09	0.26	0.02	0.07	0.06	0.01	0.43
8	Ud-17-04	n = 9	41.70	0.17	18.69	5.73	20.06	0.39	7.58	5.43	0.03	99.79
		σ	0.16	0.01	0.10	0.09	0.07	0.01	0.05	0.04	0.01	0.29
9	Ud-602	n = 13	41.30	0.18	18.61	5.75	20.07	0.39	7.60	5.51	0.03	99.44
		σ	0.14	0.01	0.11	0.12	0.09	0.01	0.07	0.03	0.01	0.18
10	Ud-35-02	n = 6	42.07	0.24	20.94	3.15	20.23	0.39	7.89	4.74	0.03	99.67
		σ	0.15	0.01	0.18	0.13	0.10	0.02	0.09	0.03	0.00	0.22
11	Ud-211-02	n = 6	42.03	0.46	18.52	5.30	20.75	0.32	7.34	5.34	0.04	100.10
		σ	0.29	0.09	0.27	0.33	0.29	0.01	0.07	0.05	0.01	0.24
12	Ud-8-07	n = 9	40.85	0.31	16.21	8.63	19.22	0.39	7.47	6.47	0.04	99.60
		σ	0.28	0.01	0.27	0.34	0.26	0.01	0.22	0.14	0.01	0.35
14	Ud-75-04	n = 9	41.42	0.20	16.24	8.60	20.13	0.32	6.95	6.16	0.11	100.13
		σ	0.27	0.01	0.20	0.10	0.11	0.01	0.07	0.08	0.26	0.34
15	Ud-334-05	n = 10	40.97	0.78	15.74	8.08	19.97	0.30	7.18	6.29	0.04	99.35
		σ	0.07	0.01	0.14	0.18	0.08	0.00	0.04	0.06	0.01	0.22
16	Ud-10-04	n = 8	42.07	0.26	21.65	2.34	20.31	0.43	8.45	4.33	0.07	99.92
		σ	0.20	0.03	0.14	0.05	0.10	0.01	0.04	0.09	0.02	0.28
12	Ud-6-07	n = 5	42.07	0.25	22.06	1.65	20.44	0.41	8.47	4.52	0.05	99.90
		σ	0.14	0.02	0.05	0.05	0.09	0.01	0.10	0.04	0.01	0.21
17	Ud-28–07	n = 8	40.99	0.01	18.77	6.28	18.90	0.44	7.68	6.48	0.01	99.55
		σ	0.31	0.01	0.16	0.11	0.32	0.03	0.20	0.10	0.01	0.48

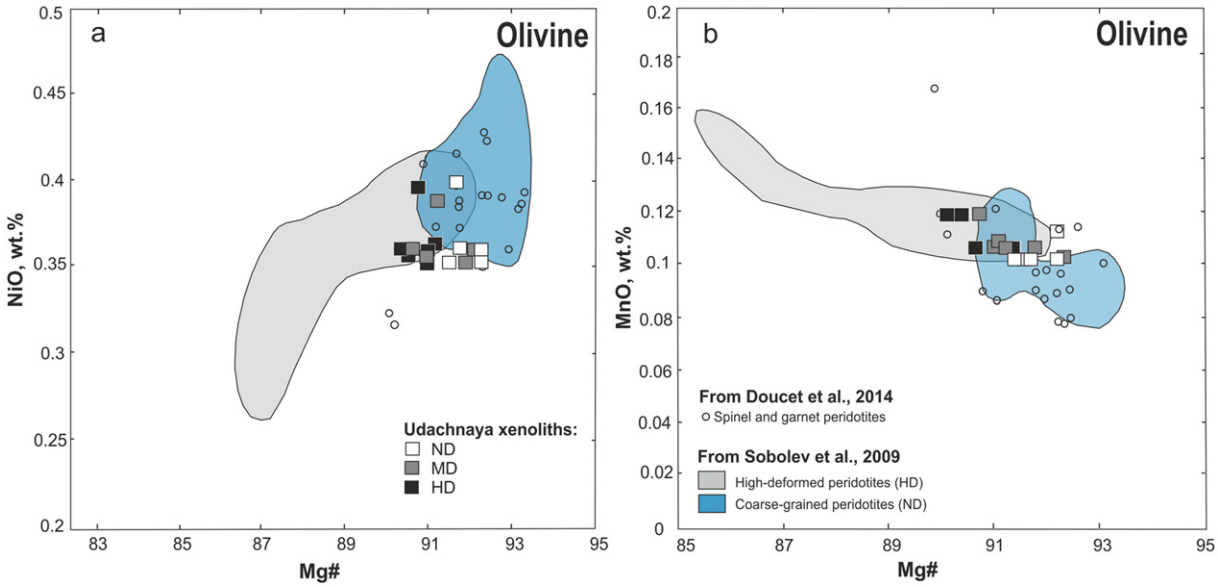

Fig. 5. Mg-number (Mg#) versus NiO and MnO in olivines from Udachnaya peridotites. Symbols as in Fig. 4.

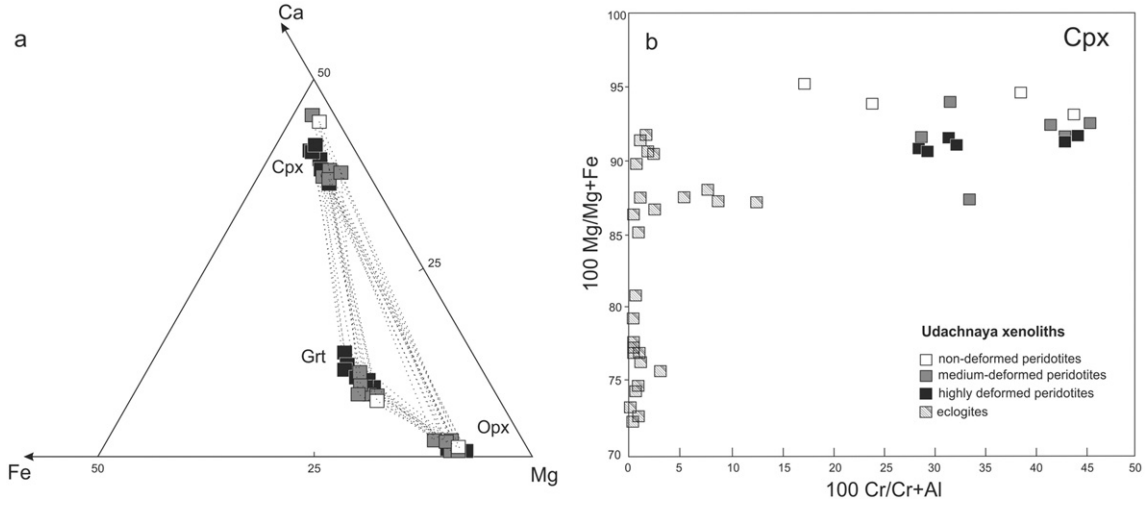

Fig. 6. Composition of pyroxenes and garnets from Udachnaya peridotites. a, Fe-Ca-Mg triangle showing three clusters of compositions for Grt, Cpx and Opx. b, Cr# vs. Mg#. Symbols as in Fig. 4.

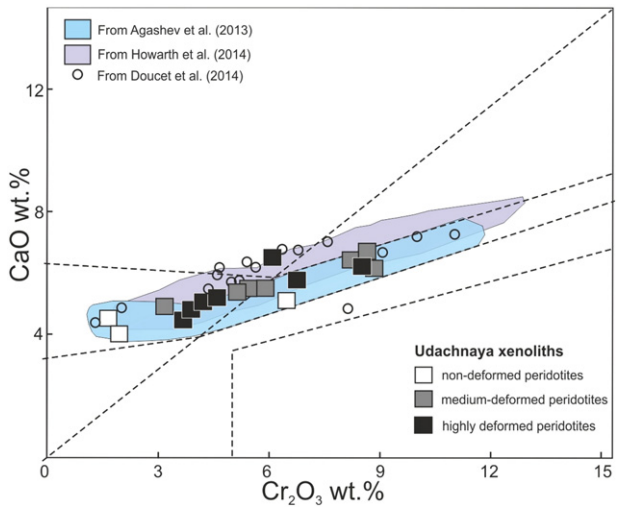

Fig. 7. Cr_2O_3 versus CaO in garnets from Udachnaya deformed peridotite xenoliths. Symbols as in Fig. 4.

olivine has several different hydroxide components. The FTIR spectra of the studied samples show characteristic absorption bands at 3490, 3510, 3570 and 3595 cm^{-1} as illustrated in Fig. 9. The bands in the 3680–3710 cm^{-1} region can be assigned to microinclusions of hydrous minerals, for example, talc or serpentine, which cannot be identified by optical observation. These bands have been detected in three samples (Ud-195-02, Ud-211-02, Ud-226-02) resulting, accordingly, in a little inaccuracy in the three calculated values of water. We excluded this band from the calculation of water content. However, that possibly resulted in a small error in the water contents calculated for these three samples as the presence of any hydrous phase definitely affected whole FTIR spectra. In general, the spectra are characterized by high absorption. The α (alpha) spectra are characterized by high absorption with electric vector (*E*) polarized parallel to *a* [100], β (beta) and γ (gamma) spectra are characterized by lower absorption with *E* parallel to *b* [010] and *c* [001], respectively. The measured H_2O contents in olivine vary from 2 ± 1 to 95 ± 52 ppm (Table 2). It is clear that olivine from highly-deformed peridotites contain more H_2O than that in the medium-deformed and non-deformed groups: 60, 22 and 8 ppm, respectively (Fig. 9).

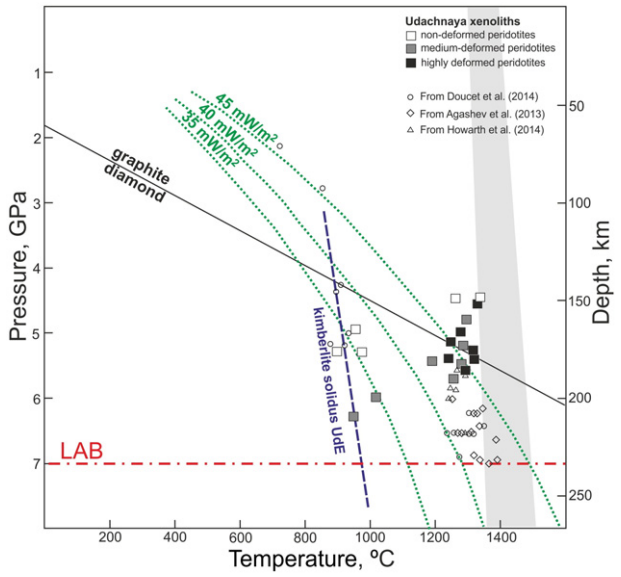

Fig. 8. Estimates of the equilibrium P-T conditions for Udachnaya peridotite xenoliths. Estimates of temperature (T, °C) by the Opx-Cpx 'solvus' (Brey and Koehler, 1990); pressure (GPa) by Ca partitioning between is from (Rudnick and Nyblade, 1999). The mantle adiabat and the 35, 40, 45 mW/m^2 conductive continental geotherms are after (Pollack and Chapman, 1977).

5.4.2. Pyroxenes

Concentrations of water in clinopyroxenes and orthopyroxenes were analyzed for 11 and 8 samples, respectively. Hydroxyl FTIR bands occur between 3000 and 3600 cm^{-1}. The FTIR spectra of diopside show three hydroxyl absorption bands with two types of pleochroism. The band at 3630 cm^{-1} is strong in direction *E* parallel to *a* (α) and direction *E* parallel to *b* (β), but weak or absent in direction *E* parallel to *c* (γ). The 3460 cm^{-1} band is mainly characterized by *E* parallel to *c* (γ) direction, while the directions of *E* parallel to *a* (α) and *E* parallel to *b* (β) are less evident (Fig. 10). The calculated contents of H_2O in clinopyroxene vary between 7 ± 2 and 71 ± 30 ppm.

The hydroxyl absorption bands in the spectra of orthopyroxenes are notably different compared to those of clinopyroxenes (Figs. 10, 11). The best peaks occur in the range from 3000 to 3600 cm^{-1}. The FTIR spectra of orthopyroxenes show characteristic absorption bands at 3060, 3300, 3410, 3510, 3545 and 3600 cm^{-1}. The calculated contents of H_2O in orthopyroxenes vary between 1 ± 0.5 and 61 ± 9 ppm. Both clinopyroxenes and orthopyroxenes show enrichment in water in the highly-deformed varieties similar to that observed in olivine (Section 5.4.1; Fig. 9). The band at 3690 cm^{-1} in the spectra of Cpx from sample Ud-1-07 and Opx from sample Ud-21-07 may be due to an inclusion of a hydrous phase. Similarly to the olivine from three samples (see Section 5.4.1).

6. Discussion

6.1. Presence and preservation of water in minerals

6.1.1. Olivine

The structural hydrogen in NAMs of deep-mantle xenoliths represents an important source of information about the content of volatiles in Earth's mantle (Bell and Rossman, 1992; Bell et al., 1995). Olivine is the most abundant mineral in the upper mantle (~60% in pyrolite), therefore, represents a key mineral for estimating bulk mantle water

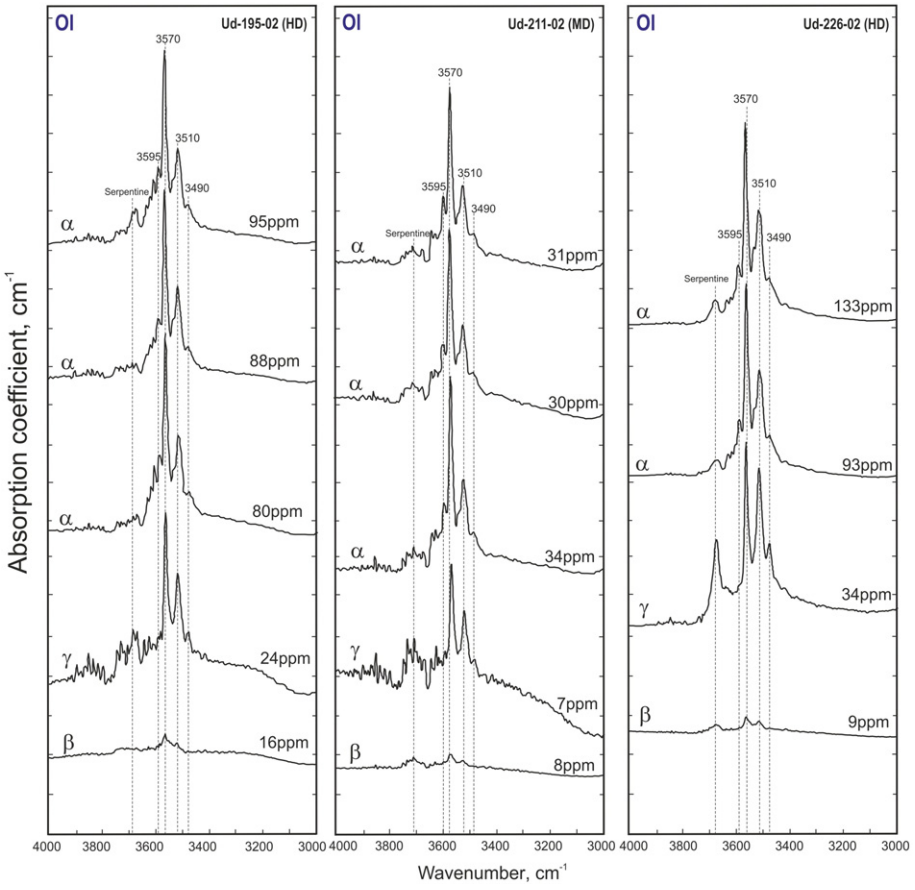

Fig. 9. Representative FTIR spectra for Udachnaya olivines in the O–H stretching frequency range. All three directions are shown as corresponding to the polarized spectra parallel to the α, β and γ directions of the olivine optical indicatrices. Dotted lines indicate peak locations.

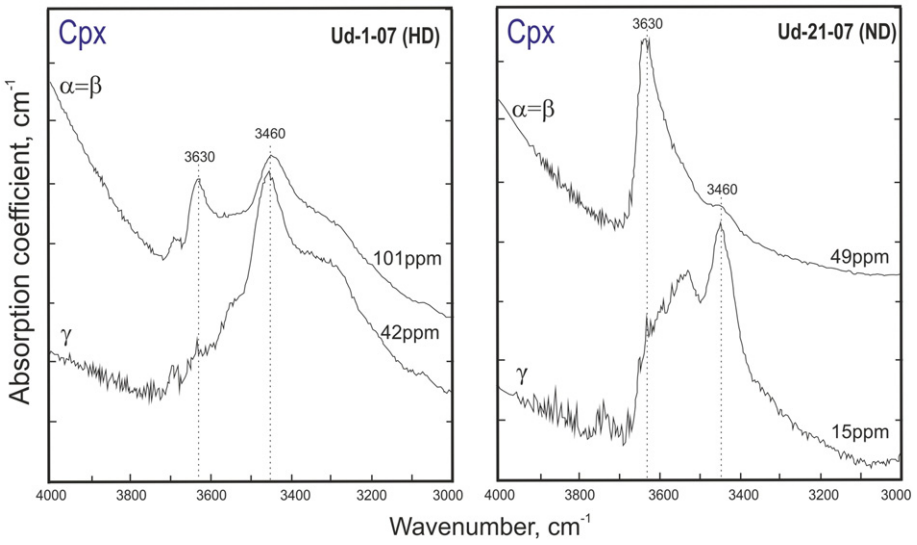

Fig. 10. Representative FTIR spectra for Udachnaya clinopyroxenes in the O—H stretching frequency range. See comments to Fig. 9.

contents. FTIR spectrometry can be used to measure the concentration of hydrogen associated with point defects in olivine crystal structure (Libowitzky and Rossman, 1997; Bell et al., 2003). Olivines from kimberlites may contain significant concentrations of water, up to 400 ppm (Miller et al., 1987; Bell et al., 2003; Matsyuk and Langer, 2004), unlike those from basaltic xenoliths, for example, San Carlos olivines from Arizona or olivines from Cenozoic alkaline basalts of the North China Craton are essentially dry containing from 0 to 1–3 ppm of water (Miller et al., 1987; Bai and Kohlstedt, 1993; Xia et al., 2013).

The amount and wave length of the bands in the hydroxyl region of infrared absorption spectra of mantle olivines are variable (Miller et al., 1987; Matsyuk and Langer, 2004). It is a common knowledge that olivine contains trace amounts of hydrogen, which is chemically bound as hydroxyl and is characterized by both intrinsic and extrinsic defects (Koch-Muller et al., 2006). Matsyuk and Langer (2004) performed a FTIR study of selected minerals from Yakutian mantle xenoliths and obtained H_2O contents of olivine varying from 4 to 350 ppm. Moreover they recognized several types of hydroxyl defects: hydroxyl groups occurring as isolated local defects (ILD) and condensed extended defects (CED), which are intrinsic to olivine structure, and non-intrinsic separate inclusions in olivine (NSI). The absence of any link between NSI and ILD/CED defects suggests that NSI may form during secondary processes, e.g., serpentinization. In general, the types of hydroxyl defects in olivine structure weakly depend on the oxygen fugacity variations (Sokol et al., 2010).

Khisina et al. (2001) studied olivine crystals from two mantle xenoliths of the Udachnaya and Obnazhyonnaya kimberlite pipes (Yakutia) by transmission electron microscopy and FTIR techniques. The olivines contain three types of nanometer-sized inclusions all of which containing hydroxyl or water: "large" inclusions carry hydrous magnesium silicates, such as 10-Å phases, lamellar defects and "small" inclusions hosting "hydrous olivine" ($Mg_{2-x}v_xSiO_4H_{2x}$, where v – is a vacancy in Mg-site).

We calculated water contents in olivine crystals using the calibration coefficients of Bell et al. (2003) (Table 2). The contents of water in the olivine grains under study are lower than those obtained earlier (up to 300 ppm, Koch-Muller et al., 2006; Doucet et al., 2014) (Fig. 12). Such an inconsistency probably comes from the overestimation of the water contents by accounting the absorption bands of serpentine or other inclusions.

Experimental data show that the solubility and the mechanism of incorporation of hydrogen depend on pressure, temperature oxygen fugacity, and water and Fe contents (Bai and Kohlstedt, 1993; Keppler, 1996; Matveev et al., 2001). For example, hydrogen content in forsterite

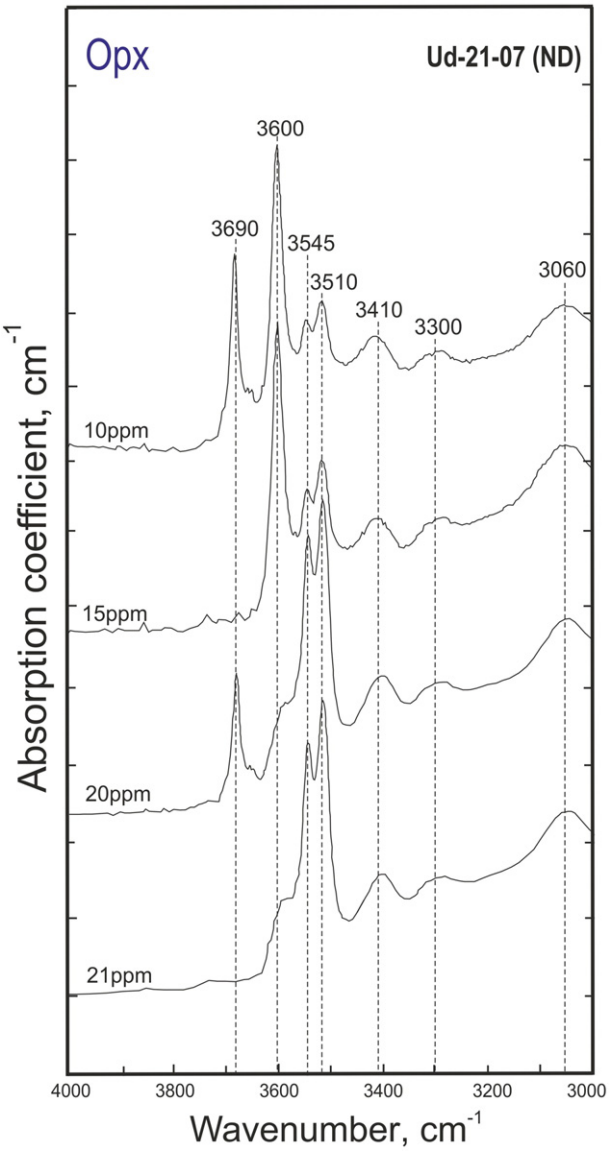

Fig. 11. Representative FTIR spectra for Udachnaya orthopyroxenes in the O—H stretching frequency range. See comments to Fig. 9.

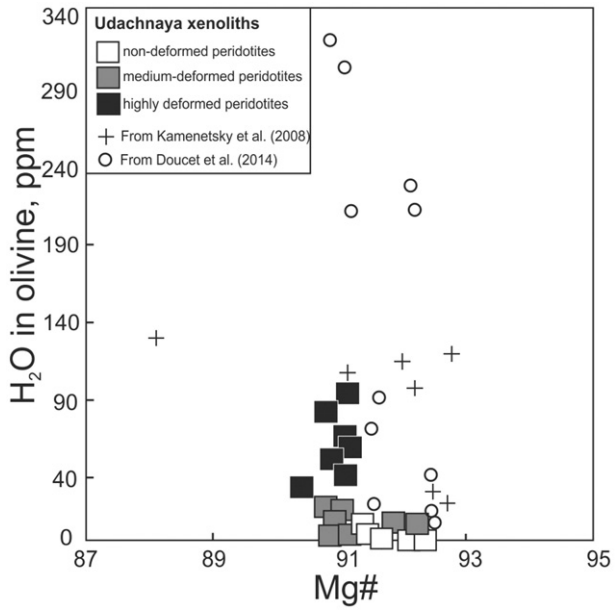

Fig. 12. Olivine water contents versus Mg# in olivine. Symbols as in Fig. 4. Data sources: Doucet et al., 2014 (filled circles), Kamenetsky et al., 2008 (crosses).

increases with pressure: the maximal concentrations of hydrogen equivalent to 0.6–0.9 wt.% H_2O were detected in forsterite synthesized at 12–14 GPa and 1200–1250 °C (Smyth et al., 2006; Litasov et al., 2007). For natural samples, no correlations have been recorded between water concentration and olivine composition, e.g., forsterite content (Fig. 12) and trace elements (Doucet et al., 2014). However, the content of water in the Udachnaya olivines under study increases with increasing degree of rock deformation. The highly deformed garnet lherzolites host olivine with higher water contents low variable Mg# (91–92), whereas the medium-deformed or non-deformed samples host olivine with lower water contents and Mg# varying in a slightly wider range (90.3–92.4; Fig. 12).

It is a common knowledge that kimberlite magma is water-rich. Therefore, the minerals of peridotite xenoliths can capture hydrogen from hosting kimberlite magma. Evidence for such a mechanism of water-enrichment comes from the diffusion profiles showing lower and higher amounts of hydrogen at the edges and in the center of mineral grains, respectively (e.g., Doucet et al., 2014). Kamenetsky et al. (2008) suggested that the cores and rims of olivine phenocrysts from kimberlites form at different conditions, at higher and lower pressures, respectively. We found no water enrichment/depletion in the olivine grains from the xenoliths under study, therefore the addition of water by host magma is unlikely. Moreover, the concentrations of H_2O in olivines from xenoliths are typically lower than those in olivine phenocrysts from Udachnaya kimberlite (Koch-Muller et al., 2006; Kamenetsky et al., 2008).

6.1.2. Pyroxenes

Although the abundance of pyroxenes in mantle xenoliths is less than 20%, the information about the content of water in those minerals is of significant importance. For example, the spinel-peridotite xenoliths of Mexico and Simcoe (USA) contain clinopyroxenes and orthopyroxenes with 140 to 528 ppm and 39 to 265 ppm of H_2O, respectively (Peslier et al., 2002). In these pyroxenes the water content increases with increasing Al_2O_3, TiO_2, CaO, Na_2O but with decreasing MgO. In addition, pyroxene reveals a negative correlation between hydrogen concentration and oxygen fugacity, probably due to the mechanism of hydrogen incorporation into pyroxene, which depends on the redox state of iron (Peslier et al., 2002). In pyroxene megacrysts the amount of water decreases with decreasing Mg/(Mg + Fe) in orthopyroxene and increases and then decreases with increasing Ca/(Ca + Mg) in clinopyroxene (Peslier, 2010).

In our study, the concentrations of water in clinopyroxenes and orthopyroxenes vary from 7 to 71 ppm and from 1 to 61 ppm, respectively (Table 2). The experimental results show that the incorporation of water into pyroxenes, like in olivines, depends on temperature, pressure, oxygen fugacity and Fe content (Ingrin et al., 1989; Skogby, 1994; Woods et al., 2000). Although our obtained data show no correlation between water content and FeO in Udachnaya pyroxenes, we can see correlation between the concentrations of water in pyroxenes and the degree of deformation: the water contents in pyroxenes increase from ND to MD and HD peridotite varieties (27, 31 and 46 ppm in Cpx and 10, 24 and 27 ppm in Opx, respectively) (Table 2).

6.2. Water equilibrium between coexisting minerals

The partition coefficients of H_2O in the minerals of Udachnaya peridotites are very variable (Table 8). The water contents shown in Table 2 were used for the calculation of partitioning coefficients. We compared the calculated coefficients with the experimentally obtained hydrogen partition coefficients of Tenner et al. (2009) and Withers et al. (2011), where the conditions of experiments, i.e. 5–6 GPa and 1200–1400 °C, were close to the equilibration conditions of most Udachnaya peridotites under study (Section 5.3; Fig. 8). The $D_{mineral/mineral}$ of Udachnaya xenoliths ranges from 0.15 to 11.88 for $D_{Ol/Opx}$, from 0.16 to 2.13 for $D_{Ol/Cpx}$ and from 0.34 to 3.86 for $D_{Opx/Cpx}$ (Table 8). The Ol/Opx water ratios (average $D_{Ol/Opx} = 1.81$) are higher than the experimental partition coefficients ($D_{Ol/Opx}$exp = 0.03–0.07) from Tenner et al. (2009). However, our calculated $D_{Ol/Opx}$ is similar to those ($D_{Ol/Opx} = 1.67$) obtained at 6 GPa by (Withers et al., 2011). Such a discrepancy between the experimental data of (Tenner et al., 2009) and (Withers et al., 2011) could be caused by the higher FeO content in the olivines from the latter study (Withers et al., 2011).

The water ratios between orthopyroxene and clinopyroxene are, in average ($D_{Opx/Cpx} = 0.88$), consistent with those determined experimentally ($D_{Opx/Cpx}$exp = 0.6–0.9) (Tenner et al., 2009). Our data are, in general, consistent with the results of (Bell and Rossman, 1992; Peslier et al., 2012), which show that clinopyroxene contains approximately twice as much water as orthopyroxene. The H_2O partition coefficients between minerals ($D_{Ol/Grt}$, $D_{Opx/Cpx}$, $D_{Cpx/Grt}$) from another set of Udachnaya peridotite xenoliths (Ragozin et al., 2014a, 2014b) are 2–5 times lower than the coefficients obtained in the frame of the present

Table 8
H_2O partition coefficients for peridotite minerals.

Sample	Rock type	DD	Ol/Cpx	Ol/Opx	Opx/Cpx
Ud-226-02	Grt-lhz	HD	1.6	2.16	0.74
Ud-1-07	Grt-lhz	HD	0.75	1.61	0.46
Ud-51-04	Grt-lhz	HD	1.61	11.88	0.14
Ud-8-04	Grt-lhz	HD	1.48	3.31	0.45
Ud-11-04	Grt-lhz	HD	2.13	3.61	0.59
Ud-195-02	Grt-lhz	HD	1.63	1.02	1.61
Ud-998-05	Grt-lhz	HD	0.46	0.9	0.51
Ud-17-04	Grt-lhz	MD	0.26	0.25	1.04
Ud-602	Grt-lhz	MD	0.44	0.37	1.2
Ud-35-02	Grt-lhz	MD	0.28	0.71	0.4
Ud-211-02	Grt-lhz	MD	0.56	1.1	0.51
Ud-8-07	Grt-lhz	MD	0.25	0.73	0.34
Ud-75-04	Grt-lhz	MD	0.57	0.15	3.86
Ud-334-05	Grt-lhz	MD	0.49	0.48	1.02
Ud-10-04	Grt-lhz	ND	0.17	0.24	0.72
Ud-21–07	Lhz	ND	0.16	0.29	0.53
Ud-6-07	Grt-lhz	ND	0.43	–	–
Ud-28–07	Grt-hrz	ND	–	2	–
Experimental data			0.03–0.04	0.03–0.07	0.6–0.9

Abbreviations: DD, degree of deformation; HD, highly deformed; MD, medium-deformed; ND, non-deformed; Grt-lhz, garnet lherzolite; Lhz, lherzolite; Grt-hrz, garnet harzburgite; experimental data from (Tenner et al., 2009).

study, however, the quality of the earlier results is doubtful since they were calculated from unpolarized FTIR spectra. Fig. 13 compares the contents of water in (a) Cpx and Opx, (b) Cpx and Ol and (c) Opx and Ol. The content of water in Opx is positively correlated with that in Cpx (Fig. 13a). Therefore, H_2O was probably in equilibrium between coexisting Opx and Cpx. Compared to the experimental data olivine is more enriched in water relative to pyroxene (Fig.13b, c). As H_2O in olivine from garnet peridotites increases the partition coefficients between pyroxenes/olivine decrease by a significant factor (around 4) at the spinel/garnet mantle facies boundary while the partition coefficient between pyroxenes remains constant (Grant et al., 2007). Our obtained partition coefficients indicate that minerals in xenoliths can deviate from the equilibrium in terms of water content, which is closely connected with different hydrogen diffusion rates over structural defects in different minerals during a possible metasomatic event (Grant et al., 2007).

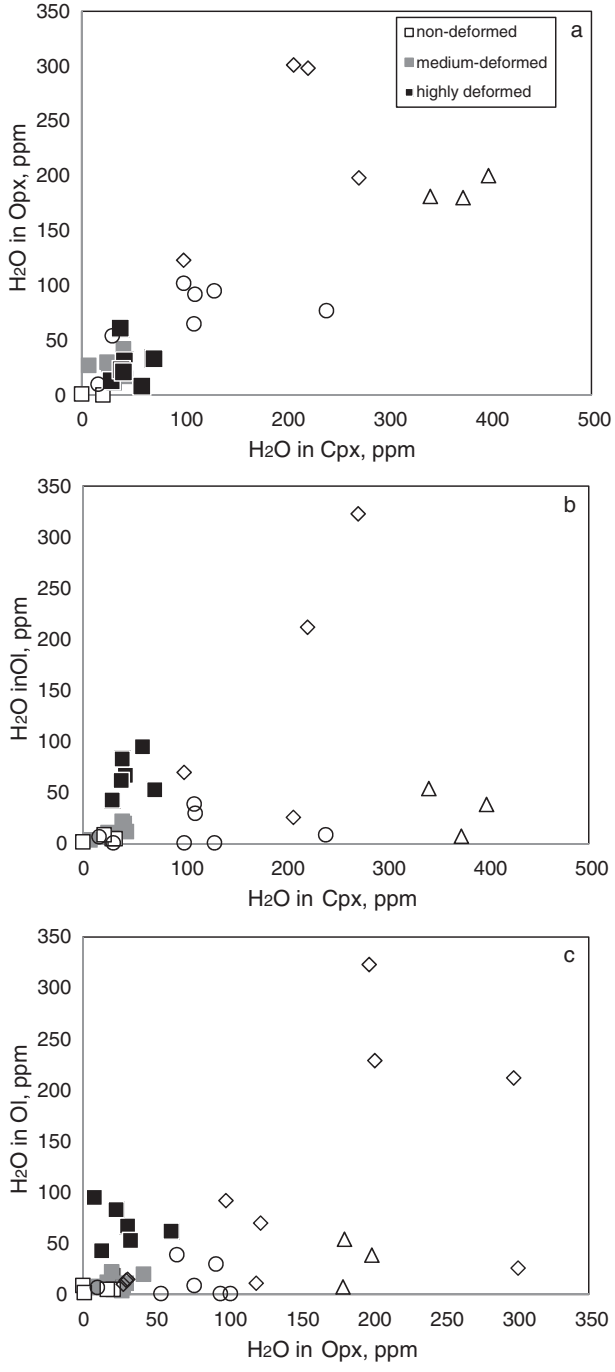

Fig. 13. Water contents in Cpx vs. Opx (a), Cpx vs. Ol (b) and Opx vs. Ol (c). Data sources: Hui et al., 2015 (open circles), Doucet et al., 2014 (open diamonds), Grant et al., 2007 (open triangles).

6.3. Water storage capacity and water controlling conditions

Taking into account the volume ratios of mineral phases in the studied xenoliths, the water contents in peridotites (whole-rock) vary over a relatively narrow range, from 1 to 64 ppm (Table 2). Fig. 14 shows two trends of whole rock water contents versus calculated temperatures in peridotites: low-temperature (800–1000 °C) and high-temperature (1100–1300 °C). The low- and high-temperature trends correspond to the water-poor and non-deformed peridotites, and water-rich and medium to highly deformed peridotites, respectively (Fig. 14). Thus, the low water content of the granular peridotite may represent its original abundance in the subcontinental lithospheric mantle (SCLM) beneath Siberia, whereas the higher water content in the deformed peridotites may indicate an enrichment caused by a metasomatic event. In any case, the water contents estimated in the Udachnaya peridotites and, in particular, in the olivines are significantly lower than the water storage capacity at 5–6 GPa and 1200-1400 °C (Bali et al., 2008; Tenner et al., 2009; Sokol et al., 2010).

According to Hirschmann et al. (2005), H_2O storage capacity is a maximal mass fraction of H_2O that can be retained in a mineral at a given temperature and pressure. This is different from H_2O solubility in a mineral, which requires $X_{H2O} = 1$ in coexisting fluid (Sokol et al., 2010). This restriction should be taken into account when discussing water contents in natural and synthetic minerals. Recent models of the formation of cratonic mantle consider peridotites as high-degree melt residues extracted either by shallow melting in the spinel stability field and subsequent subduction (Canil, 2004; Simon et al., 2007) or by deep melt extraction by plume activity (Griffin et al., 2003). The melting regimes of the cratonic mantle are typically reconstructed using the concentrations of FeO, CaO, Al_2O_3 and MgO in mantle peridotites (e.g., Herzberg, 2004; Ionov and Hofmann, 2007; Wittig et al., 2008). Fig. 4 shows a trend between the Bulk Silicate Earth and cratonic peridotite compositions, which indicate a residual nature of the peridotites under study (e.g., Herzberg, 2004). The experimental results on mantle

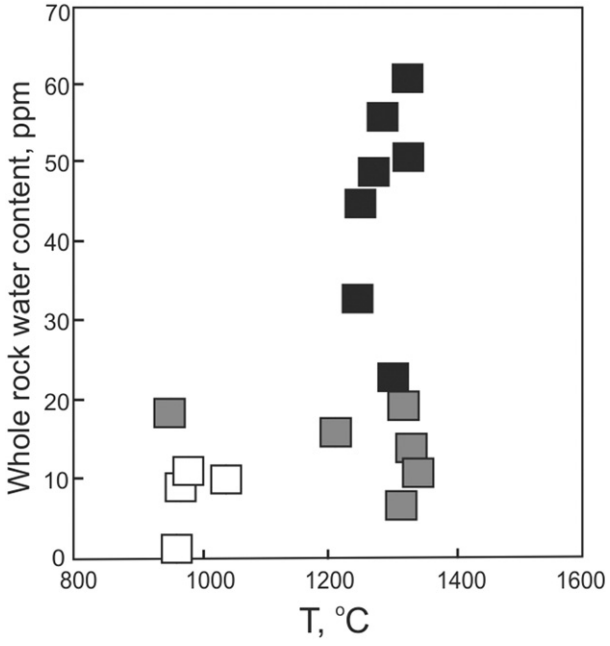

Fig. 14. Whole-rock water content versus temperature calculated using the Opx-Cpx 'solvus' (Brey and Koehler, 1990). Symbols as in Fig. 4.

melting from Herzberg (2004) show that FeO contents are sensitive to the initial depth of melting. High-pressure residues have much lower FeO (6–7.5 wt.%) than the residues formed at lower pressures (7.5–9 wt.% FeO). Deformed and non-deformed peridotites of the Udachnaya have relatively high FeO contents of 8.02–9.75 measured for whole-rock samples and therefore can be attributed to low-pressure residues.

Water behaves highly incompatibly during mantle melting. Experiments show strong influence of water on melting temperature and stable phase relations of partially molten peridotite (Kushiro, 1972; Green, 1973; Mysen and Boettcher, 1975; Gaetani and Grove, 1998). After partial melting, the peridotite residue should be essentially free of water, therefore water enrichment would be connected with secondary metasomatic processes in the SCLM. However in some cases residual peridotites have relatively high water content after partial melting with following metasomatism (Hao et al., 2014). Denis et al. (2015) have also noted that hydrous metasomatism does not effect on water content in nominally anhydrous minerals (NAMs) in the peridotite xenoliths of Ray Pic volcano, Central massif, France. Moreover they showed that the volatile-rich melts percolation do not influence on water content in the NAMs. This fact is difficult to explain because of highly incompatible behavior of water in the upper mantle minerals.

Hydrogen solubility in olivine coexisting with oxidized H_2O-CO_2-bearing fluid/melt was studied in details by Litasov et al. (2009) and Sokol et al. (2013a). Those researchers have shown that at 6.3 GPa and 1400 °C the content of H_2O in the olivine coexisting with H_2O-CO_2-bearing media decreases significantly and is less than 100–400 ppm at $CO_2/(CO_2 + SiO_2) = 0.4–0.8$ (the latter values correspond to carbonatitic melt) (Sokol et al., 2013b). Thus, the low contents of H_2O in peridotite minerals (olivine: 2 ± 1–95 ± 52 ppm, orthopyroxene: 1 ± 0.5–61 ± 9 ppm, clinopyroxene: 7 ± 2–71 ± 30 ppm) can be caused by the action of carbonatite melts in the Siberian SCLM. Indeed, interaction with carbonatite melts must be fingerprinted in the major and trace element composition of the peridotite minerals. Evidence for the presence of carbonatite melts in the Siberian SCLM comes from carbonates in diamond inclusions and from peridotite xenoliths showing signs of wehrlitization (see below) (Kamenetsky et al., 2004; Zedgenizov et al., 2004, 2007; Kamenetsky et al., 2009; Agashev et al., 2013; Pokhilenko et al., 2015; Sharygin et al., 2015).

In addition, the lower concentrations of water in mantle-depth olivines could be linked with its loss during magma/mineral ascent to Earth's surface, which is a typical feature of the minerals from xenoliths in Cenozoic alkaline basalts (Ingrin and Skogby, 2000; Demouchy and Mackwell, 2006; Xia et al., 2013; Li et al., 2015). However, taking into account the high water content of kimberlite magma the minerals of Udachnaya xenoliths unlikely lost their water during the transportation to the surface. The established contents of hydrogen in peridotite olivines ranging (2–95 ppm) are lower than those in typical olivine phenocrysts from kimberlites (up to 100–350 ppm) (Koch-Muller et al., 2006; Kamenetsky et al., 2008).

6.4. Deformation, metasomatism and geodynamic implications

The presented collection of xenoliths from the Udachnaya pipe includes three types of rocks classified according to the degree of their deformation: non-deformed (garnet lherzolite, garnet harzburgite, lherzolite and dunite), medium-deformed and highly deformed (garnet-lherzolites only in both cases; Table 2). The degree of deformation seems to be linked or depend on the concentration of water and on the P-T parameters. For example, the content of water in whole-rock xenoliths and in olivines notably increases from non-deformed to medium- and highly deformed peridotites: 6, 16 and 45 ppm (peridotites) and 4, 12 and 60 in average, respectively (Table 2). The redox and thermal state of the mantle beneath Udachnaya has been studied by many researchers (e.g., Goncharov et al., 2012; Yaxley et al., 2012). But in this paper we made the first attempt to link temperature and degree of deformation. Our results show that the calculated temperatures increase with the increasing degree of deformation (Fig. 14). On the contrary, the contents of Cr_2O_3 and CaO in garnets of all groups of xenoliths, non-deformed, medium-deformed and highly deformed, are close to each other suggesting that they were not affected by the subsequent metasomatism. All this suggests a heterogeneous distribution of water in the cratonic mantle beneath the central Siberian Craton, which resulted in mantle metasomatism.

Percolative metasomatism is a typical way of mantle modification in the SCLM, which has been recorded at numerous localities and from many collections of mantle xenoliths worldwide (e.g., Menzies et al., 1987; Ionov et al., 1993; Griffin et al., 1999; Kamenetsky et al., 2004; Smith et al., 2004). A range of models of metasomatic modification of Siberian cratonic roots has been proposed based on Udachnaya xenoliths as well (Agashev et al., 2013; Doucet et al., 2014; Howarth et al., 2014; Pokhilenko et al., 2015). The metasomatism probably controls the composition of lithospheric mantle, diamond formation and petrogenesis of kimberlitic and other magmas (Pokhilenko et al., 2015).

There have been proposed several models for the deformation of peridotites. According to O'Reilly and Griffin (2010), deformed peridotites are refertilized parts of the Archean cratonic mantle. Local variations in water concentration may initiate shearing (Skemer et al., 2010, 2013; Wang et al., 2013). In addition, the deformation can be caused by uprising mantle plumes (Green and Gueguen, 1974), by the introduction of asthenospheric melts (Ehrenberg, 1979), and by the shear heating at the lithosphere-asthenosphere boundary (LAB) at which the temperature jumps up to 1400 °C (Kennedy et al., 2002). Some researchers think that the formation of deformed peridotites can be linked to the crystallization of megacrysts (Harte and Hawkesworth, 1989; Burgess and Harte, 2004; Solov'eva et al., 2008). Accordingly, the formation of highly deformed peridotites can be a regional event triggered by plume activity and metasomatism at the LAB, or a local event forming those rocks at weakened zones near kimberlite channels and vein systems.

Since a combination of structural and chemical instabilities cannot be maintained in mantle conditions for a long time, the formation of deformed peridotites can be connected with a single thermal event (see the peridotite xenoliths matching the 45 mW/m^2 geotherm in Fig. 8), which triggered the generation of kimberlite magma at the base of the cratonic mantle and its subsequent intrusion (Agashev et al., 2010). Such a model implies that the deformation was probably coeval to a certain stage of kimberlite metasomatism.

Fig. 15 shows two models of metasomatism of the lithospheric mantle at cratonic roots and its connection with water contents in peridotites. The plume model agrees with the widely manifested intra-plate magmatism within the Siberian craton and the surrounding Central Asian Orogenic Belt (CAOB), which formed many Devonian to Cenozoic intra-plate basaltic fields in the CAOB (Kuzmin et al., 2010; Safonova et al., 2015) and kimberlite fields in the Siberian Craton (Pokhilenko et al., 2015; Sharygin et al., 2015).

The vein model implies the generation of kimberlite melts within local segments at the LAB. It suggests that each magmatic vein system ever existed around a kimberlite pipe was unique and formed in weakened lithosphere zones. Thus, the formation of deformed peridotites and diamondiferous depleted peridotites by metasomatism, but by different metasomatic events, is spatially restricted by a narrow 1–10 km wide zone. The vein model may be applied to explain the formation of diamonds and diamondiferous peridotites, but is hardly applicable for discussing the formation of deformed peridotites. Evidence for this model comes from zonal trace-element patterns and isotopic characteristics of minerals from xenoliths (Malkovets et al., 2007; Doucet et al., 2014).

Novella et al. (2015) reported a small amount of water in diamond mineral inclusions (<1 ppm in garnet to 5 ppm in olivine). They concluded that the H_2O contents in the minerals are representative and that peridotite was in equilibrium with fluids that produced diamonds. On the contrary, Taylor et al. (2016) suggested higher water content based on olivine from inclusions in Udachnaya diamond (2–34 ppm)

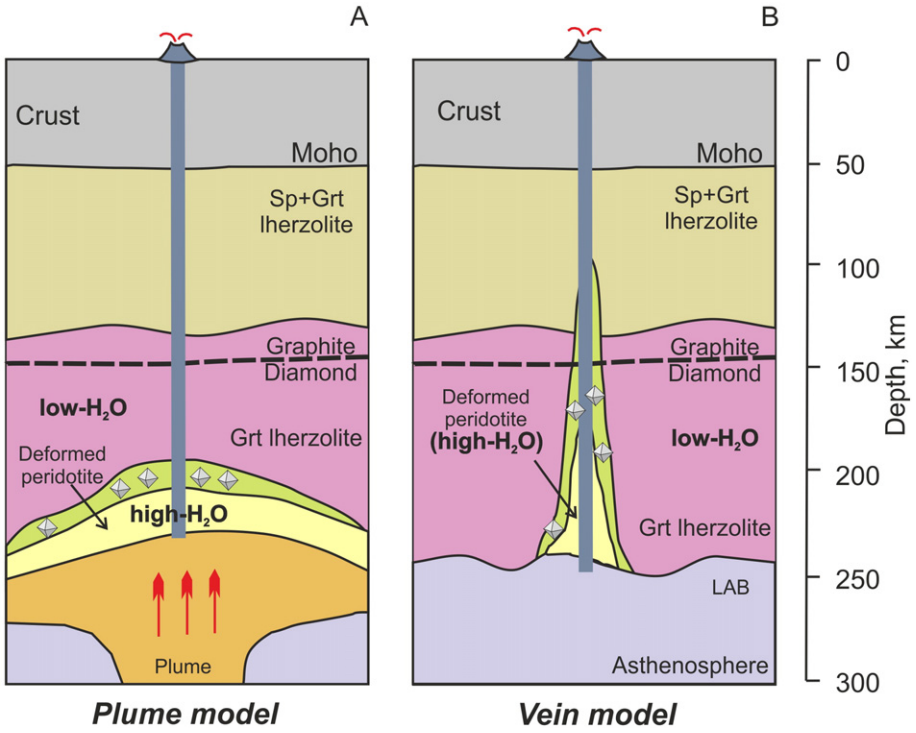

Fig. 15. Models for mantle metasomatism at cratonic roots accounting water contents in peridotites. A, the plume model implying metasomatism in a large subcratonic region (Howarth et al., 2014; Pokhilenko et al., 2015; Sharygin et al., 2015). B, the vein model implying metasomatism at local weak zones beneath kimberlites (Malkovets et al., 2007). Red arrows are for fluid/melt flows and gray octahedra show the areas of diamond crystallization. LAB, lithosphere-asthenosphere boundary; Sp, spinel.

and concluded that H_2O content in NAMs inclusions in diamonds is representative for the ancient mantle at the time of diamond formation. Still both studies indicate essentially dry peridotites at the lithosphere roots of the Siberian craton. The high H_2O content of NAMs in mantle xenoliths is not indicative for the Siberian SCLM, but reflects later metasomatism (Doucet et al., 2014) and suggests that diamonds formed before the event of metasomatism, which affected the deformed peridotite. We think that the formation of deformed peridotite could be caused by hydrated fluids, which origin is consistent rather with hydrous-silicic then carbonatitic medium (Zedgenizov et al., 2004). The interaction of essentially carbonatitic fluids with peridotites would cause depletion by orthopyroxene and formation of wehrlitic series, which is not the case for most deformed peridotites. However, sparse deformed peridotites carry signatures of wehrlitization (e.g., Sharygin et al., 2015).

Metasomatism is often discussed in relation to intra-plate magmatism of OIB type, because, for example, the parental melts of Ti-Nb-LREE enriched intra-plate basalts cannot be derived by direct melting of spinel or garnet peridotites (Kamber and Collerson, 2000; Dasgupta et al., 2007; Safonova and Santosh., 2014). The intra-plate continental magmatism, which is typically manifested as kimberlite pipes and dikes, fields of OIB-type basalts and bi-modal volcanic series, and spatially related to rift structures, is often attributed to mantle plumes generated either at the core–mantle boundary or in the mantle transition zone (Maruyama and Okamoto, 2007; Howarth et al., 2014; Pokhilenko et al., 2015; Safonova et al., 2015; Sharygin et al., 2015). Recent geological, petrologic and geophysical studies in Asia made a basis for the model of volatile-bearing plumes generated in the transition zone, which are related to the subduction of hydrated and carbonated oceanic slab and continental crust materials to the deep mantle. The plumes are triggered by the melting of subducted MORB in presence of the volatiles, water and CO_2, which are stored by NAMs and DHMSs, and by the accumulation of U-Th-K rich continental crust material (Kawai et al., 2013; Safonova et al., 2015). Post-Miocene Asia is surrounded by two giant subduction zones, western Pacific and India-Sumatra, which supply the oceanic and continental materials to the mantle and generate hydrous-carbonate plumes, which, in turn, produce intra-continental basaltic and bi-modal volcanic fields of central and east Asia. In Neoproterozoic-Cambrian time, the Siberian continent was surrounded by several continuous subduction systems from the west and south, which have been found and studied in folded belts surrounding the Siberian Craton (Fig. 1) including the Yenisei range and Transbaikalia (e.g., Turkina et al., 2012; Kröner et al., 2014; Safonova, 2017). Those subduction zones could also supply water and carbonates into the sub-cratonic mantle and induce its metasomatism.

7. Conclusions

Nineteen samples of peridotite xenoliths (garnet lherzolite, lherzolite, dunite and garnet harzburgite) from the Udachnaya kimberlite pipe of the Yakutian diamondiferous province were investigated for whole-rock and mineral composition, PT-parameters and water content (FTIR). The peridotites have fresh appearance and possess granular, porphyroclastic, mosaic-porphyroclastic and mylonitic textures. Based on the degree of the deformation the peridotites were divided into three groups: non-deformed, medium-deformed and highly deformed.

The pressure and temperature estimates range from 4.6 to 6.3 GPa and from 913 to 1324 °C, respectively. The non-deformed and medium-deformed peridotites formed at 5.0–6.3 GPa and 913–1039 °C matching the 35 mW/m^2 conductive continental geotherm. The highly deformed peridotites formed at 4.8–5.6 GPa and 1245–1324 °C matching the 45 mW/m^2 conductive continental geotherm.

The water contents in garnet peridotite xenoliths vary from 2 ± 1 to 95 ± 52 ppm in olivine, from 1 ± 0.5 to 61 ± 9 ppm in orthopyroxene, from 7 ± 2 to71 ± 30 ppm in clinopyroxene. The amount of water in garnets is negligible. Based on the modal proportions of mineral phases in the xenoliths, the water contents in peridotites were estimated to vary over a narrow range from <1 to 64 ppm. The amount of water in the

mantle xenoliths is well correlated with the deformation degree: highly deformed peridotites show highest water contents (64 ppm) and those medium-deformed and non-deformed contain ca. 1 ppm of H_2O.

The variably low water contents suggest a heterogeneous distribution of water beneath the mantle, which can be connected with metasomatism of essentially dry diamondiferous cratonic roots by hydrous and carbonatitic agents, and its related hydration and carbonation of peridotite accompanied by oxidation and dissolution of diamonds. This model of heterogenous water distribution in the cratonic mantle beneath the Udachnaya pipe is consistent with the models of mantle plumes or veined mantle structures proposed based on a trace element study of similar xenolithic suits.

Mantle metasomatism beneath the Siberian Craton and its triggered kimberlite magmatism could be induced by mantle enrichment in volatiles (H_2O, CO_2) supplied by numerous subduction zones which surrounded the Siberian continent in Neoproterozoic-Cambrian time.

Acknowledgements

We appreciate very much the comments from Prof. Q. Xia and an anonymous reviewer as well as the handling editor for their comments and suggestions which all helped us to improve the manuscript to a significant degree. Special thanks to Prof. V. Shatsky who provided the collection of peridotite samples. The work was supported, in parts, by state assignment project (VIII.67.3.1.), scientific project of IGM SB RAS Lab 211 (no. 0330-2016-0003) and the Russian Foundation for Basic Research (projects no. 15-55-50033; 15-55-53029; 16-35-00317, 16-05-00313). Geochemical studies were performed in the frame of a laboratory project of the Ministry of Education and Science of the Russian Federation (no. 14.B25.31.0032 and no. 14.Y26.31.0018). Contribution to IGCP#592.

Appendix A. Supplementary data

Supplementary data to this article can be found online at doi:10.1016/j.gr.2016.09.011.

References

Afanas'ev, V.P., Zinchuk, N.N., Logvinova, A.M., 2009. Distribution of placer diamonds related to Precambrian sources. Geology of Ore Deposits 51 (8), 675–683.

Agashev, A.M., Pokhilenko, N.P., Tolstov, A.V., Polyanichko, V.G., Mal'kovets, V.G., Sobolev, N.V., 2004. New age data on kimberlites from the Yakutian diamondiferous province. Doklady Earth Sciences 399, 1142–1145.

Agashev, A.M., Pokhilenko, N.P., Cherepanova, Y.V., Golovin, A.V., 2010. Geochemical evolution of rocks at the base of the lithospheric mantle: evidence from study of xenoliths of deformed peridotites from kimberlite of the Udachnaya pipe. Doklady Earth Sciences 432 (4), 746–749.

Agashev, A.M., Ionov, D.A., Pokhilenko, N.P., Golovin, A.V., Cherepanova, Y., Sharygin, I.S., 2013. Metasomatism in lithospheric mantle roots: constraints from whole-rock and mineral chemical composition of deformed peridotite xenoliths from kimberlite pipe Udachnaya. Lithos 160-161, 201–215.

Bai, Q., Kohlstedt, D., 1993. Effects of chemical environment on the solubility and incorporation mechanism for hydrogen in olivine. Physics and Chemistry of Minerals 19, 460–471.

Bali, E., Bolfan-Casanova, N., Koga, K.T., 2008. Pressure and temperature dependence of H solubility in forsterite: an implication to water activity in the Earth interior. Earth and Planetary Science Letters 268, 354–363.

Bell, D.R., Rossman, G.R., 1992. Water in Earth's mantle - the role of nominally anhydrous minerals. Science 255, 1391–1397.

Bell, D.R., Ihinger, P.D., Rossman, G.R., 1995. Quantitative analysis of trace OH in garnet and pyroxenes. American Mineralogist 80, 465–474.

Bell, D.R., Rossman, G.R., Maldner, J., Endisch, D., Rauch, F., 2003. Hydroxide in olivine: a quantitative determination of the absolute amount and calibration of the spectrum. Journal of Geophysical Research 108, 1–9.

Bernstein, S., Kelemen, P.B., Hanghoi, K., 2007. Consistent olivine Mg# in cratonic mantle reflects Archean mantle melting to the exhaustion of orthopyroxene. Geology 35, 459–462.

Boyd, F.R., 1989. Compositional distinction between oceanic and cratonic lithosphere. Earth and Planetary Science Letters 96, 15–26.

Boyd, F.R., Pokhilenko, N.P., Pearson, D.G., Mertzman, S.A., Sobolev, N.V., Finger, L.W., 1997. Composition of the Siberian cratonic mantle: evidence from Udachnaya peridotite xenoliths. Contributions to Mineralogy and Petrology 128 (2–3), 228–246.

Brey, G.P., Koehler, T., 1990. Geothermobarometry in four-phase lherzolites II. New thermobarometers, and practical assessment of existing thermobarometers. Journal of Petrology 31, 1353–1378.

Burgess, S.R., Harte, B., 2004. Tracing lithosphere evolution through the analysis of heterogeneous G9–G10 garnets in peridotite xenoliths, II: REE chemistry. Journal of Petrology 45, 609–633.

Canil, D., 2004. Mildly incompatible elements in peridotites and the origins of mantle lithosphere. Lithos 77, 375–393.

Dasgupta, R., Hirschmann, M.M., Smith, N.D., 2007. Partial melting experiments of peridotite + CO2 at 3 GPa and genesis of alkalic ocean island basalts. Journal of Petrology 48, 2093–2124.

Davis, G.L., Sobolev, N.V., Kharkiv, A.D., 1980. New data on the age of Yakutian kimberlites (U-Pb zircon method). Doklady Earth Sciences 254 (1), 175–179.

Demouchy, S., Mackwell, S., 2006. Mechanisms of hydrogen incorporation and diffusion in iron-bearing olivine. Physics and Chemistry of Minerals 33, 347–355.

Denis, C., Alard, O., Demouchy, S., 2015. Water content and hydrogen behaviour during metasomatism in the uppermost mantle beneath Ray Pic volcano (Massif Central, France). Lithos 236-237, 256–274.

Doucet, L.S., Peslier, A.H., Ionov, D.A., Brandon, A.D., Golovin, A.V., Goncharov, A.G., Ashchepkov, I.V., 2014. High water contents in the Siberian cratonic mantle linked to metasomatism: an FTIR study of Udachnaya peridotite xenoliths. Geochimica et Cosmochimica Acta 137, 159–187.

Egorov, K.N., Kornilova, V.P., Safronov, A.F., Filippov, N.D., 1986. Micaceous kimberlite from the Udacgnaia-Vostochnaia pipe. Doklady Akademii Nauk SSSR 291 (1), 199–202.

Ehrenberg, S.N., 1979. Garnetiferous ultramafic inclusions in minette from the Navajo volcanic field. Proc. of the 2nd Intern. Kimberlite Conference. American Geophysical Union Vol. 2, pp. 213–226.

Gaetani, G.A., Grove, T.L., 1998. The influence of water on melting of mantle peridotite. Contributions to Mineralogy and Petrology 131, 323–346.

Goncharov, A.G., Ionov, D.A., Doucet, L.S., Pokhilenko, L.N., 2012. Thermal state, oxygen fugacity and C-O-H fluid speciation in cratonic lithospheric mantle: new data on peridotite xenoliths from Udachnaya kimberlite, Siberia. Earth and Planetary Science Letters 357-358, 99–110.

Grant, K.J., Kohn, S.C., Brooker, R.A., 2007. The partitioning of water between olivine, orthopyroxene and melt synthesized in the system albite–forsterite–H_2O. Earth and Planetary Science Letters 260, 227–241.

Green, D.H., 1973. Experimental melting studies on a model upper mantle composition at high pressure under water-saturated and water-undersaturated conditions. Earth and Planetary Science Letters 19, 37–53.

Green, D.H., Gueguen, Y., 1974. Origin of kimberlite pipes by diapiric upwelling in the upper mantle. Nature 249, 617–620.

Griffin, W.L., Shee, S.R., Ryan, C.G., Win, T.T., Wyatt, B.A., 1999. Harzburgite to lherzolite and back again: metasomatic processes in ultramafic xenoliths from the Wesselton kimberlite, Kimberley, South Africa. Contributions to Mineralogy and Petrology 134 (2–3), 232–250.

Griffin, W.L., O'Reilly, S.Y., Abe, N., Aulbach, S., Davies, R.M., Pearson, N.J., Doyle, B.J., Kivi, K., 2003. The origin and evolution of Archean lithospheric mantle. Precambrian Research 127, 19–41.

Hao, Y.T., Xia, Q.K., Liu, S.C., Feng, M., Zhang, Y.P., 2012. Recognizing juvenile and relict lithospheric mantle beneath the North China Craton: combined analysis of H_2O, major and trace elements and Sr-Nd isotope compositions of clinopyroxenes. Lithos 149, 136–145.

Hao, Y.T., Xia, Q.K., Li, Q.W., Chen, H., Feng, M., 2014. Partial melting control of water contents in the Cenozoic lithospheric mantle of the Cathaysia block of South China. Chemical Geology 380, 7–19.

Hao, Y.T., Xia, Q.K., Jia, Z.B., Zhao, Q.C., Li, P., Feng, M., Liu, S.C., 2016. Regional heterogeneity in the water content of the Cenozoic lithospheric mantle of Eastern China. Journal of Geophysical Research 121, 517–537.

Harte, B., 1977. Rock nomenclature with particular relation to deformation and recrystallization textures in olivine-bearing xenoliths. Journal of Geology 85, 279–288.

Harte, B., Hawkesworth, C.J., 1989. Mantle domains and mantle xenoliths. Special Publication. Geological Society of Australia 14 (2), 649–686.

Herzberg, C., 2004. Geodynamic information in peridotite petrology. Journal of Petrology 45, 2507–2530.

Hirschmann, M.M., Abaud, C., Withers, A.C., 2005. Storage capacity of H_2O in nominally anhydrous minerals in the upper mantle. Earth and Planetary Science Letters 236, 167–181.

Howarth, G.H., Barry, P.H., Pernet-Fisher, J.F., Baziotis, I.P., Pokhilenko, N.P., Pokhilenko, L.N., Bodnar, R.J., Taylor, L.A., Agashev, A.M., 2014. Superplume metasomatism: evidence from Siberian mantle xenoliths. Lithos 184-187, 209–224.

Hui, H.J., Pesleir, A.H., Rudnick, R.L., Simonetti, A., Neal, C.R., 2015. Plume-cratonic lithopshere interaction recorded by water and other trace elements in peridotite xenoliths from the Labait volcano, Tanzania. Geochemistry, Geophysics, Geosystems 16, 1687–1710.

Ilupin, I.P., 1990. Geochemistry of Kimberlites. Nedra, Moscow (352 pp. in Russian).

Ingrin, J., Skogby, H., 2000. Hydrogen in nominally anhydrous upper-mantle minerals: concentration levels and implications. European Journal of Mineralogy 12, 543–570.

Ingrin, J., Latrous, K., Doukhan, J.C., Doukhan, N., 1989. Water in diopsides: an electron microscopy and infrared spectroscopy study. European Journal of Mineralogy 1, 327–341.

Ionov, D.A., Hofmann, A.W., 2007. Depth of formation of sub-continental off-craton peridotites. Earth and Planetary Science Letters 261, 620–634.

Ionov, D.A., Dupuy, C., O'Reilly, S.Y., Kopylova, M.G., Genshaft, Y.S., 1993. Carbonated peridotite xenoliths from Spitsbergen: implications for trace element signature of mantle carbonate metasomatism. Earth and Planetary Science Letters 119, 283–297.

Jean, M.M., Taylor, L.A., Howarth, G.H., Peslier, A.H., Fedele, L., Bodnar, R.J., Guan, Y., Doucet, L.S., Ionov, D.A., Logvinova, A.M., Golovin, A.V., Sobolev, N.V., 2016. Olivine inclusions in Siberian diamonds and mantle xenoliths: contrasting water and trace-element contents. Lithos http://dx.doi.org/10.1016/j.lithos.2016.07.023.
Kamber, B.S., Collerson, K.D., 2000. Zr/Nb systematics of oceanic island basalts reassessed – the case for binary mixing. Journal of Petrology 41, 1007–1021.
Kamenetsky, M.B., Sobolev, A.V., Kamenetsky, V.S., Maas, R., Danyushevsky, L.V., Thomas, R., Pokhilenko, N.P., Sobolev, N.V., 2004. Kimberlite melts rich in alkali chlorides and carbonates: a potent metasomatic agent in the mantle. Geology 32, 845–848.
Kamenetsky, V.S., Kamenetsky, M.B., Sobolev, A.V., Golovin, A.V., Demouchy, S., Faure, K., Sharygin, V.V., Kuzmin, D.V., 2008. Olivine in the Udachnaya-East kimberlite (Yakutia, Russia): types, compositions and origins. Journal of Petrology 49 (4), 823–839.
Kamenetsky, V.S., Kamenetsky, M.B., Weiss, Y., Navon, O., Nielsen, T.F.D., Mernagh, T.P., 2009. How unique is the Udachnaya-East kimberlite? Comparison with kimberlites from the Slave Craton (Canada) and SW Greenland. Lithos 112S, 334–346.
Kawai, K., Yamamoto, S., Tsuchiya, T., Maruyama, S., 2013. The second continent: existence of granitic continental materials around the bottom of the mantle transition zone. Geoscience Frontiers 4 (1), 1–6.
Kennedy, L.A., Russell, K.J., Kopylova, M.G., 2002. Mantle shear zones revisited: the connection between the cratons and mantle dynamics. Geology 30 (5), 419–422.
Kent, A.J.R., Rossman, G.R., 2002. Hydrogen, lithium, and boron in mantle-derived olivine: the role of coupled substitutions. American Mineralogist 87, 1432–1436.
Keppler, H., 1996. The investigation of phase transitions by electronic absorption spectroscopy. Physics and Chemistry of Minerals 23, 288–296.
Khar'kiv, A.D., Zuenko, V.V., Zinchuk, N.N., Kruchkov, A.I., Ukhanov, V.A., Bogatykh, M.M., 1991. Kimberlite Petrochemistry. TCNIGRI Publishing House, Yakutsk (302 pp. in Russian).
Khisina, N.R., Wirth, R., Andrut, M., Ukhanov, A.V., 2001. Extrinsic and intrinsic mode of hydrogen occurrence in natural olivines: FTIR and TEM investigation. Physics and Chemistry of Minerals 28, 291–301.
Kinny, P.D., Griffin, B.J., Heaman, L.M., Brakhfogel, F.F., Spetsius, Z.V., 1997. SHRIMP U-Pb ages of perovskite from Yakutian kimberlites. Journal of Geology and Geophysics 38 (1), 91–99.
Koch-Muller, M., Matsyuk, S.S., Rhede, D., Wirth, R., Khisina, N., 2006. Hydroxyl in mantle olivine xenocrysts from the Udachnaya kimberlite pipe. Physics and Chemistry of Minerals 33, 276–287.
Koehler, T., Brey, G.P., 1990. Calcium exchange between olivine and clinopyroxene calibrated as a geothermobarometer for natural peridotites from 2 to 60 kb with applications. Geochimica et Cosmochimica Acta 54, 2375–2388.
Kopylova, M.G., Kostrovitsky, S.I., Egorov, K.N., 2013. Salts in southern Yakutian kimberlites and the problem of primary alkali kimberlite melts. Earth-Science Reviews 119, 1–16.
Kornilova, V.P., Egorov, K.N., Safronov, A.F., Filippov, N.D., Zaitsev, A.I., 1998. Monticellite kimberlite from the Udachnaya–East pipe and some aspects of the evolution of kimberlite melts. Russian Geology 1, 48–51.
Kröner, A., Kovach, V., Belousova, E., Hegner, E., Armstrong, R., Dolgopolova, A., Seltmann, R., Alexeiev, D.V., Hoffmann, J.E., Wong, J., Sun, M., Cai, K., Wang, T., Tong, Y., Wilde, S.A., Degtyarev, K.E., Rytsk, E., 2014. Reassessment of continental growth during the accretionary history of the Central Asian Orogenic Belt. Gondwana Research 25, 103–125.
Kurosawa, M., Yurimoto, H., Sueno, S., 1997. Patterns in the hydrogen and trace element compositions of mantle olivines. Physics and Chemistry of Minerals 24, 385–395.
Kushiro, I., 1972. Effect of water on the composition of magmas formed at high pressures. Journal of Petrology 13, 311–334.
Kuzmin, M.I., Yarmolyuk, V.V., Kravchinsky, V.A., 2010. Phanerozoic hot spot traces and paleogeographic reconstructions of the Siberian continent based on interaction with the African large low shear velocity province. Earth-Science Reviews 102 (1), 29–59.
Lavrent'ev, Y.G., Korolyuk, V.N., Usova, L.V., Nigmatulina, E.N., 2015. Electron probe microanalysis of rock-forming minerals with a JXA-8100 electron probe microanalyzer. Russian Geology and Geophysics 56 (10), 1428–1436.
Lee, C.T.A., 2006. Geochemical/petrologic constraints on the origin of cratonic mantle. Archean Geodynamics and Environments, pp. 89–114.
Li, P., Xia, Q.K., Deloule, E., Chen, H., Gu, X.Y., Feng, M., 2015. Temporal variation of H_2O content in the lithospheric mantle beneath the eastern North China Craton: implications for the destruction of cratons. Gondwana Research 28 (1), 276–287.
Libowitzky, E., Rossman, G.R., 1997. An IR absorption calibration for water in minerals. American Mineralogist 82, 1111–1115.
Litasov, K.D., Ohtani, E., Kagi, H., Jacobsen, S.D., Ghosh, S., 2007. Temperature dependence and mechanism of hydrogen incorporation in olivine at 12.5–14.0 GPa. Geophysical Research Letters 34 (16).
Litasov, K.D., Shatskiy, A.F., Katsura, T., Ohtani, E., 2009. Water solubility in forsterite at 8–14 GPa. Doklady Earth Sciences 425 (2), 432–435.
Malkovets, V.G., Griffin, W.L., O'Reilly, S.Y., Wood, B.J., 2007. Diamond, subcalcic garnet, and mantle metasomatism: kimberlite sampling patterns define the link. Geology 35 (4), 339–342.
Maruyama, S., Okamoto, K., 2007. Water transportation from the subducting slab into the mantle transition zone. Gondwana Research 11 (1), 148–165.
Matsyuk, S.S., Langer, K., 2004. Hydroxyl in olivines from mantle xenoliths in kimberlites of the Siberian platform. Contributions to Mineralogy and Petrology 147, 413–437.
Matsyuk, S.S., Langer, K., Hosch, A., 1998. Hydroxyl defects in garnets from mantle xenoliths in kimberlites of the Siberian platform. Contributions to Mineralogy and Petrology 132, 163–179.
Matveev, S., O'Neill, H.S.C., Ballhaus, C., Taylor, W., Green, D., 2001. Effect of silica activity on OH^- IR spectra of olivine: implications for low-aSiO_2 mantle metasomatism. Journal of Petrology 42, 721–729.
McDonough, W.F., Rudnick, R.L., 1998. Mineralogy and composition of the upper mantle. Reviews in Mineralogy 37, 139–164.
McDonough, W.F., Sun, S.S., 1995. The composition of the Earth. Chemical Geology 120 (3), 223–253.
Mei, S., Kohlstedt, D.L., 2000a. Influence of water on plastic deformation of olivine aggregates: 1. Diffusion creep regime. Journal of Geophysical Research: Solid Earth 105 (B9), 21457–21469.
Mei, S., Kohlstedt, D.L., 2000b. Influence of water on plastic deformation of olivine aggregates: 2. Dislocation creep regime. Journal of Geophysical Research: Solid Earth 105 (B9), 21471–21481.
Menzies, M.A., Rogers, N., Tindle, A., Hawkesworth, C.J., 1987. Metasomatic and Enrichment Processes in Lithospheric Peridotites, an Effect of Asthenosphere-Lithosphere Interaction. pp. 313–361.
Miller, G.H., Rossman, G.R., Harlow, G.E., 1987. The natural occurrence of hydroxide in olivine. Physics and Chemistry of Minerals 14, 461–472.
Mosenfelder, J.L., Deligne, N.I., Asimow, P.D., Rossman, G.R., 2006. Hydrogen incorporation in olivine from 2–12GPa. American Mineralogist 91, 285–294.
Mysen, B.O., Boettcher, A.L., 1975. Melting of hydrous upper mantle. I. Phase equilibria of a natural peridotite at high pressures and high temperatures as a function of controlled activities of water, hydrogen and carbon dioxide. Journal of Petrology 16, 520–548.
Novella, D., Bolfan-Casanova, N., Nestola, F., Harris, J.W., 2015. H_2O in olivine and garnet inclusions still trapped in diamonds from the Siberian craton: implications for the water content of cratonic lithosphere peridotites. Lithos 230, 180–183.
O'Reilly, S.Y., Griffin, W.L., 2010. The continental lithosphere–asthenosphere boundary: can we sample it? Lithos 120 (1), 1–13.
Passchier, C.W., Trouw, R.A.J., 2005. Microtectonics (366 pp.).
Pearson, D.G., Canil, D., Shirey, S.B., 2003. Mantle samples included in volcanic rocks: xenoliths and diamonds. Treatise on Geochemistry 2, 171–275.
Peslier, A.H., 2010. A review of water contents of nominally anhydrous natural minerals in the mantles of Earth, Mars and the Moon. Journal of Volcanology and Geothermal Research 197 (1), 239–258.
Peslier, A.H., Bizimis, M., 2015. Water in Hawaiian peridotite minerals: a case for a dry metasomatized oceanic mantle lithosphere. Geochemistry, Geophysics, Geosystems 16, 1211–1232.
Peslier, A.H., Luhr, J.F., Post, J., 2002. Low water contents in pyroxenes from spinel-peridotites of the oxidized, sub-arc mantle wedge. Earth and Planetary Science Letters 201, 69–86.
Peslier, A.H., Woodland, A.B., Wolff, J.A., 2008. Fast kimberlite ascent rates estimated from hydrogen diffusion profiles in xenolithic olivines from Southern Africa. Geochimica et Cosmochimica Acta 72, 2711–2722.
Peslier, A.H., Woodland, A.B., Bell, D.R., Lazarov, M., Lapen, T.J., 2012. Metasomatic control of water contents in the Kaapvaal cratonic mantle. Geochimica et Cosmochimica Acta 97, 213–246.
Pokhilenko, N.P., Agashev, A.M., Litasov, K.D., Pokhilenko, L.N., 2015. Carbonatite metasomatism of peridotite lithospheric mantle: implications for diamond formation and carbonatite-kimberlite magmatism. Russian Geology and Geophysics 56 (1), 280–295.
Pollack, H.N., Chapman, D.S., 1977. On the regional variation of heat flow, geotherms, and lithospheric thickness. Tectonophysics 38 (3), 279–296.
Ragozin, A.L., Karimova, A.A., Litasov, K.D., Zedgenizov, D.A., Shatsky, V.S., 2014a. Water content in minerals of mantle xenoliths from the Udachnaya pipe kimberlites (Yakutia). Russian Geology and Geophysics 55, 425–439.
Ragozin, A.L., Zedgenizov, D.A., Shatskii, V.S., Orihashi, Y., Agashev, A.M., Kagi, H., 2014b. U-Pb age of rutile from the eclogite xenolith of the Udachnaya kimberlite pipe. Doklady Earth Sciences 457 (1), 861–864.
Rudnick, R.L., Nyblade, A.A., 1999. The thickness and heat production of Archean lithosphere: constraints from xenolith thermobarometry and surface heat flow. Mantle Petrology: Field Observations and High Pressure Experimentation: A Tribute to Francis R. (Joe) Boyd 6, pp. 3–12.
Safonova, I.Y., 2017. Juvenile versus recycled crust in the Central Asian Orogenic Belt: implications from ocean plate stratigraphy, blueschist belts and intra-oceanic arcs. Gondwana Research 47, 6–27.
Safonova, I., Santosh., M., 2014. Accretionary complexes in the Asia-Pacific region: tracing archives of ocean plate stratigraphy and tracking mantle plumes. Gondwana Research 25, 126–158.
Safonova, I., Maruyama, S., Litasov, K., 2015. Generation of hydrous-carbonated plumes in the mantle transition zone linked to tectonic erosion and subduction. Tectonophysics 662, 454–471.
Schmadicke, E., Gose, J., Reinhardt, J., Will, T.M., Stalder, R., 2015. Garnet in cratonic and non-cratonic mantle and lower crustal xenoliths from Southern Africa: composition, water incorporation and geodynamic constraints. Precambrian Research 270, 285–299.
Sharygin, I.S., Litasov, K.D., Shatskiy, A., Golovin, A.V., Ohtani, E., Pokhilenko, N.P., 2015. Melting phase relations of the Udachnaya-East Group-I kimberlite at 3.0–6.5 GPa: experimental evidence for alkali-carbonatite composition of primary kimberlite melts and implications for mantle plumes. Gondwana Research 28 (4), 1391–1414.
Simon, N.S.C., Carlson, R.W., Pearson, D.G., Davies, G.R., 2007. The origin and evolution of the Kaapvaal cratonic lithospheric mantle. Journal of Petrology 48, 589–625.
Skemer, P., Warren, J.M., Kelemen, P.B., Hirth, G., 2010. Structural and rheological evolution of a mantle shear zone. Journal of Petrology 51 (1–2), 43–53.
Skemer, P., Warren, J.M., Hansen, L.N., Hirth, G., Kelemen, P.B., 2013. The influence of water and LPO on the initiation and evolution of mantle shear zones. Earth and Planetary Science Letters 375, 222–233.
Skogby, H., 1994. OH incorporation in synthetic clinopyroxene. American Mineralogist 79, 240–249.

Smelov, A.P., Timofeev, V.F., 2007. The age of the North Asian Cratonic basement: an overview. Gondwana Research 12 (3), 279–288.
Smith, C.B., Sims, K., Chimuka, L., Duffin, A., Beard, A.D., Townend, R., 2004. Kimberlite metasomatism at Murowa and Sese pipes, Zimbabwe. Lithos 76 (1), 219–232.
Smyth, J.R., Frost, D.J., Nestola, F., Holl, C.M., Bromiley, G., 2006. Olivine hydration in the deep upper mantle: effects of temperature and silica activity. Geophysical Research Letters 33 (15).
Sobolev, N.V., 1977. Deep-seated Inclusions in Kimberlites and the Problem of the Composition of the Upper Mantle. American Geophysical Union, Washington, DC, p. 279.
Sobolev, N.V., Lavrent'ev, Y.G., Pokhilenko, N.P., Usova, L.V., 1973. Chrome-rich garnets from kimberlites of Yakutia and their paragenesis. Contributions to Mineralogy and Petrology 40, 39–52.
Sobolev, N.V., Logvinova, A.M., Zedgenizov, D.A., Pokhilenko, N.P., Malygina, E.V., Kuzmin, D.V., Sobolev, A.V., 2009. Petrogenetic significance of minor elements in olivines from diamonds and peridotite xenoliths from kimberlites of Yakutia. Lithos 112, 701–713.
Sokol, A.G., Palyanov, Y.N., Kupriyanov, I.N., Litasov, K.D., Polovinka, M.P., 2010. Effect of oxygen fugacity on the H_2O storage capacity of forsterite in the carbon-saturated systems. Geochimica et Cosmochimica Acta 74, 4793–4806.
Sokol, A.G., Kupriyanov, I.N., Palyanov, Y.N., Kruk, A.N., Sobolev, N.V., 2013a. Melting experiments on the Udachnaya kimberlite at 6.3–7.5 GPa: implications for the role of H_2O in magma generation and formation of hydrous olivine. Geochimica et Cosmochimica Acta 101, 133–155.
Sokol, A.G., Kupriyanov, I.N., Palyanov, Y.N., 2013b. Partitioning of H_2O between olivine and carbonate–silicate melts at 6.3 GPa and 1400 °C: implications for kimberlite formation. Earth and Planetary Science Letters 383, 58–67.
Solov'eva, L.V., Lavrent'ev, Y.G., Egorov, K.N., Kostrovitskii, S.I., Korolyuk, V.N., Suvorova, L.F., 2008. The genetic relationship of the deformed peridotites and garnet megacrysts from kimberlites with asthenospheric melts. Russian Geology and Geophysics 49, 207–224.
Spetsius, Z.V., Belousova, E.A., Griffin, W.L., O'Reilly, S.Y., Pearson, N.J., 2002. Archean sulfide inclusions in Paleozoic zircon megacrysts from the Mir kimberlite, Yakutia: implications for the dating of diamonds. Earth and Planetary Science Letters 199 (1), 111–126.
Taylor, L.A., Logvinova, A.M., Howarth, G.H., Liu, Y., Peslier, A.H., Rossman, G.R., Guan, Y., 2016. Low water contents in diamond mineral inclusions: proto-genetic origin in a dry cratonic lithosphere. Earth and Planetary Science Letters 433, 125–132.
Tenner, T.J., Hirschmann, M.M., Withers, A.C., Hervig, R.L., 2009. Hydrogen partitioning between nominally anhydrous upper mantle minerals and melt between 3 and 5 GPa and applications to hydrous peridotite partial melting. Chemical Geology 262 (1–2), 42–56.
Turkina, O.M., Berezhnaya, N.G., Lepekhina, E.N., Kapitonov, I.N., 2012. U–Pb (SHRIMP II), Lu–Hf isotope and trace element geochemistry of zircons from high-grade metamorphic rocks of the Irkut terrane, Sharyzhalgay Uplift: implications for the Neoarchaean evolution of the Siberian Craton. Gondwana Research 21 (4), 801–817.
Walter, M.J., 1998. Melting of garnet peridotite and the origin of komatiite and depleted lithosphere. Journal of Petrology 39, 29–60.
Wang, Q., Xia, Q.K., O'Reilly, S.Y., Griffin, G.L., Beyer, E.E., Brueckner, H.K., 2013. Pressure- and stress-induced fabric transition in olivine from peridotites in the Western Gneiss Region (Norway): implications for mantle seismic anisotropy. Journal of Metamorphic Geology 31, 91–111.
Withers, A.C., Hirschmann, M.M., Tenner, T.J., 2011. The effect of Fe on olivine H_2O storage capacity: consequences for H_2O in the Martian mantle. American Mineralogist 96 (7), 1039–1053.
Wittig, N., Pearson, D.G., Webb, M., Ottley, C.J., Irvine, G.J., Kopylova, M., Jensen, S.M., Nowell, G.V., 2008. Origin of cratonic lithospheric mantle roots: a geochemical study of peridotites from the North Atlantic craton, West Greenland. Earth and Planetary Science Letters 274, 24–33.
Woods, C.S., Mackwell, S., Dyar, D., 2000. Hydrogen in diopside: diffusion profiles. American Mineralogist 85, 480–487.
Xia, Q.K., Hao, Y.T., Li, P., Deloule, E., Coltorti, M., Dallai, L., Yang, X.Z., Feng, M., 2010. Low water content of the Cenozoic lithospheric mantle beneath the eastern part of the North China Craton. Journal of Geophysical Research 115, B07207. http://dx.doi.org/10.1029/2009 JB006694.
Xia, Q.K., Hao, Y.T., Liu, S.C., Gu, X.Y., Feng, M., 2013. Water contents of the Cenozoic lithospheric mantle beneath the western part of the North China Craton: peridotite xenolith constraints. Gondwana Research 23 (1), 108–118.
Yang, X.-Z., Xia, Q.-K., Deloule, E., Dallai, L., Fan, Q.C., Feng, M., 2008. Water in minerals of the continental lithospheric mantle and overlying lower crust: a comparative study of peridotite and granulite xenoliths from the North China craton. Chemical Geology 256, 33–45.
Yaxley, G.M., Berry, A.J., Kamenetsky, V.S., Woodland, A.B., Golovin, A.V., 2012. An oxygen fugacity profile through the Siberian Craton – Fe K-edge XANES determinations of $Fe^{3+}/\sum Fe$ in garnets in peridotite xenoliths from the Udachnaya East kimberlite. Lithos 140-141, 142–151.
Yudin, D.S., Tomilenko, A.A., Travin, A.V., Agashev, A.M., Pokhilenko, N.P., Orihashi, Y., 2014. The age of Udachnaya-East kimberlite: U/Pb and $^{40}Ar/^{39}Ar$ data. Doklady Earth Sciences 455 (1), 288–290.
Zedgenizov, D.A., Kagi, H.K., Shatsky, V.S., Sobolev, N.V., 2004. Carbonatitic melts in cuboid diamonds from Udachnaya kimberlite pipe (Yakutia): evidence from vibrational spectroscopy. Mineralogical Magazine 68, 61–73.
Zedgenizov, D.A., Ragozin, A.L., Shatsky, V.S., 2007. Composition of diamond formation environment: data of study of microinclusions in natural diamonds. Zapiski RMO 136 (7), 159–172.
Zinchuk, N.N., Spetsius, Z.V., Zuenko, V.V., Zuev, V.M., 1993. Kimberlite Pipe Udachnaya. Novosibirsk University, Novosibirsk, p. 146.